Isomer spectroscopy in ^{133}Ba and high-spin structure of ^{134}Ba

L. Kaya,[1,*] A. Vogt,[1] P. Reiter,[1] M. Siciliano,[2,3,4] N. Shimizu,[5] Y. Utsuno,[5,6] H.-K. Wang,[7] A. Gargano,[8] L. Coraggio,[8] N. Itaco,[8,9] K. Arnswald,[1] D. Bazzacco,[10] B. Birkenbach,[1] A. Blazhev,[1] A. Bracco,[11] B. Bruyneel,[4] L. Corradi,[3] F. C. L. Crespi,[11] G. de Angelis,[3] M. Droste,[1] J. Eberth,[1] A. Esmaylzadeh,[1] E. Farnea,[10,†] E. Fioretto,[3] C. Fransen,[1] A. Gadea,[12] A. Giaz,[11] A. Görgen,[13,4] A. Gottardo,[3] K. Hadyńska-Klęk,[3] H. Hess,[1] R. Hirsch,[1] P. R. John,[14] J. Jolie,[1] A. Jungclaus,[15] V. Karayonchev,[1] L. Kornwebel,[1] W. Korten,[4] S. Leoni,[11] L. Lewandowski,[1] S. Lunardi,[2,10] R. Menegazzo,[10] D. Mengoni,[2,10] C. Michelagnoli,[16] T. Mijatović,[17] G. Montagnoli,[2,10] D. Montanari,[2,10] C. Müller-Gatermann,[1] D. Napoli,[3] Zs. Podolyák,[18] G. Pollarolo,[19] F. Recchia,[2,10] J.-M. Régis,[1] N. Saed-Samii,[1] E. Şahin,[13] F. Scarlassara,[2,10] K. Schomacker,[1] M. Seidlitz,[1] B. Siebeck,[1] P.-A. Söderström,[20] A. M. Stefanini,[3] O. Stezowski,[21] S. Szilner,[17] B. Szpak,[22] E. Teruya,[23] C. Ur,[10] J. J. Valiente-Dobón,[3] K. Wolf,[1] K. Yanase,[23] N. Yoshinaga,[23] and K. O. Zell[1]

[1]*Institut für Kernphysik, Universität zu Köln, D-50937 Köln, Germany*
[2]*Dipartimento di Fisica e Astronomia, Università di Padova, I-35131 Padova, Italy*
[3]*Istituto Nazionale di Fisica Nucleare, Laboratori Nazionali di Legnaro, I-35020 Legnaro, Italy*
[4]*Institut de Recherche sur les lois Fondamentales de l'Univers – IRFU, CEA/DSM, Université de Paris-Saclay, F-91191 Gif-sur-Yvette Cedex, France*
[5]*Center for Nuclear Study, The University of Tokyo, Hongo, Bunkyo-ku, Tokyo 113-0033, Japan*
[6]*Advanced Science Research Center, Japan Atomic Energy Agency, Tokai, Ibaraki 319-1195, Japan*
[7]*College of Physics and Telecommunication Engineering, Zhoukou Normal University, Henan 466000, People's Republic of China*
[8]*Istituto Nazionale di Fisica Nucleare, Sezione di Napoli, I-80126 Napoli, Italy*
[9]*Dipartimento di Matematica e Fisica, Università degli Studi della Campania "Luigi Vanvitelli," I-8110 Caserta, Italy*
[10]*Istituto Nazionale di Fisica Nucleare, Sezione di Padova, I-35131 Padova, Italy*
[11]*Dipartimento di Fisica, Università di Milano and INFN Sezione di Milano, I-20133 Milano, Italy*
[12]*Instituto de Física Corpuscular, CSIC-Universidad de Valencia, E-46071 Valencia, Spain*
[13]*Department of Physics, University of Oslo, P. O. Box 1048 Blindern, N-0316 Oslo, Norway*
[14]*Institut für Kernphysik, Technische Universität Darmstadt, D-64289 Darmstadt, Germany*
[15]*Instituto de Estructura de la Materia, CSIC, Madrid, E-28006 Madrid, Spain*
[16]*Institut Laue-Langevin (ILL), 38042 Grenoble Cedex 9, France*
[17]*Ruđer Bošković Institute, HR-10 002 Zagreb, Croatia*
[18]*Department of Physics, University of Surrey, Guildford, Surrey GU2 7XH, United Kingdom*
[19]*Dipartimento di Fisica Teorica dell'Università di Torino and INFN, I-10125 Torino, Italy*
[20]*Extreme Light Infrastructure-Nuclear Physics (ELI-NP), 077125 Bucharest-Magurele, Romania*
[21]*Université de Lyon, Université Lyon-1, CNRS/IN2P3, UMR5822, IPNL, F-69622 Villeurbanne Cedex, France*
[22]*Henryk Niewodniczański Institute of Nuclear Physics PAN, PL-31342 Kraków, Poland*
[23]*Department of Physics, Saitama University, Saitama City 338-8570, Japan*

(Received 24 May 2019; published 14 August 2019)

The transitional nuclei ^{134}Ba and ^{133}Ba are investigated after multinucleon transfer employing the high-resolution Advanced GAmma Tracking Array coupled to the magnetic spectrometer PRISMA at the Laboratori Nazionali di Legnaro, Italy, and after fusion-evaporation reaction at the FN tandem accelerator of the University of Cologne, Germany. The $J^\pi = 19/2^+$ state at 1942 keV in ^{133}Ba is identified as an isomer with a half-life of 66.6(20) ns corresponding to a $B(E1)$ value of $7.7(4) \times 10^{-6}\, e^2\,\mathrm{fm}^2$ for the $J^\pi = 19/2^+$ to $J^\pi = 19/2^-$ transition. The level scheme of ^{134}Ba above the $J^\pi = 10^+$ isomer is extended to approximately 6 MeV. A pronounced backbending is observed at $\hbar\omega = 0.38$ MeV along the positive-parity yrast band. The results are compared to the high-spin systematics of the $Z = 56$ isotopes. Large-scale shell-model calculations employing the GCN50:82, SN100PN, SNV, PQM130, Realistic SM, and EPQQM interactions reproduce the experimental findings and elucidate the structure of the high-spin states. The shell-model calculations employing the GCN50:82 and PQM130 interactions reproduce alignment properties and provide detailed insight into the microscopic origin of this phenomenon in transitional ^{134}Ba.

DOI: 10.1103/PhysRevC.100.024323

*Corresponding author: levent.kaya@ikp.uni-koeln.de
†Deceased.

I. INTRODUCTION

Excitations in nuclei around mass $A \approx 130$ arise from the complex interplay of single-particle and collective degrees of freedom. Quasiparticle excitations play a key role for the presence of yrast-trap isomers. Several shell-model interactions are available for the description of neutron-rich $A \approx 130$ nuclei such as GCN50:82 [1,2], SN100PN [3], SNV [4], PQM130 [5,6], and Realistic SM [7,8] including the configuration space for proton and neutrons $0g_{7/2}$, $1d_{5/2}$, $1d_{3/2}$, $s_{1/2}$, and $0h_{11/2}$ orbitals. Calculated transition probabilities between states formed from these orbitals, especially of hindered transitions, are of particular interest for tests of all components of effective interactions, such as proton-proton, neutron-neutron, and proton-neutron correlations. However, the description of transition probabilities in this valence space is limited in the sense that $E1$ transitions cannot be evaluated since only the $h_{11/2}$ orbital acts as an intruder-parity orbital. Recent interactions have been driven by studies of excitations across the $N = 82$ neutron shell incorporating the two neutron orbits $\nu 1f_{7/2}$ and $\nu 2p_{3/2}$. For example, the recently developed extended pairing plus quadrupole-quadrupole force with monopole corrections model (EPQQM) interaction provides an extended cross-shell description of the $Z \geqslant 50$, $N \leqslant 82$ region [9].

A. Isomers along $N = 77$ isotones

Along the $N = 77$ chain from ^{127}Sn to ^{137}Nd, $J^\pi = 19/2^+$ isomers are observed in almost all isotones beside ^{129}Te and they were extensively studied in the past. Starting from semimagic ^{127}Sn, Pinston *et al.* [10] identified a $J^\pi = 19/2^+$ isomer with a half-life of 4.5(3) μs, decaying via a low-energy 17-keV $E2$ transition toward the $J^\pi = 15/2^+$ state. Furthermore, a higher-lying $J^\pi = 23/2^+$ isomer was reported in ^{127}Sn (0.9(3) μs [11]). The seniority $\nu = 3$ multiplet is completed by the observation of a $J^\pi = (27/2^-)$ isomer with a half-life of 0.25(3) μs [11]. So far, only in ^{129}Te below ^{137}Nd the $J^\pi = 19/2^+$ state remained unobserved. A $J^\pi = 23/2^+$ isomers ($T_{1/2} = 33(3)$ ns [12]) is known in ^{129}Te. Adding four protons, the level scheme of ^{131}Xe was recently extended to approximately 5 MeV [13]. The first $J^\pi = 19/2^+$ state at 1805 keV, decaying via a 189.2-keV γ ray into the $J^\pi = 19/2^-$ state, has been identified as an isomer with an adopted half-life of 14(3) ns [14].

The data on low-spin states in ^{133}Ba originate from earlier work employing β decay [15], (d, p) [16], and (n, γ) reactions [17]. The $J^\pi = 11/2^-$ neutron-hole isomer at 288 keV with a half-life of 38.93(10) h has been known to be the bandhead of the negative-parity yrast band since the 1940s [18]. First results on states above the $J^\pi = 11/2^-$ isomer were reported by Gizon *et al.* [19] employing a ^{12}C + ^{124}Sn reaction. Excited states were observed up to 2.5-MeV excitation energy, among them a delayed γ-ray cascade with energies of 83, 681, and 889 keV deexciting an isomeric state at 1942 keV. In accordance with the level scheme of ^{131}Xe, ^{135}Ce, and ^{137}Nd a spin of $J^\pi = 19/2^+$ was assigned to this state. However, a precise half-life of the 1942-keV state was not evaluated; the half-life was constrained to be between 2 and 5 ns. Later, the level scheme was significantly extended by Juutinen *et al.* [20], using ^{13}C-induced reactions and the NORDBALL γ-ray array. In total, nine collective bands up to 7 MeV were observed. Moreover, it was concluded that the half-life of the 1942-keV state has to be much longer than the reported value in Ref. [19]. According to intensity correlations and a comparison with the $T_{1/2} = 52(6)$ ns $J^\pi = 5^-$ isomer in ^{134}Ba [21], a half-life of 40–50 ns was suggested by the authors of Ref. [20].

Above ^{133}Ba, approaching the $Z = 64$ subshell closure, isomeric $J^\pi = 19/2^+$ states are established in ^{135}Ce at $E_x = 2125$ keV ($T_{1/2} = 8.2(4)$ ns [22]) and in ^{137}Nd at $E_x = 2223.4$ keV (1–4 ns [23]). All known $J^\pi = 19/2^+$ isomers from ^{131}Xe to ^{137}Nd decay through strong $E1$ transitions.

B. High-spin structures of $Z = 56$ isotopes and $N = 78$ isotones

The combined contribution of neutron holes in the $N = 82$ core and proton particles in the high-$h_{11/2}$ orbital gives rise to a plethora of high-spin structures with multi-quasiparticle character. Backbending and upbending phenomena in the positive-parity yrast bands of even-even Ba isotopes with mass $A \leqslant 132$ were systematically investigated in the past. Experimental data show the presence of two aligned S bands [24] very close in energy. While one band can be assigned to quasineutron alignment, the other can be assigned to proton alignment [25–32]. The description of such collective phenomena within the shell model is quite demanding. Therefore, the majority of theoretical investigations of such systems were performed within collective models like the interacting boson model [33–35], mean-field methods [36,37], or the cranked shell model [38,39]. However, Ba isotopes have come within reach of untruncated shell-model calculations and, thus, are benchmarks for the predictive power of shell-model calculations [40–42], more specifically, the interplay between single-particle and collective excitations is subject of individual orbitals and interactions.

Similarly to the $J^\pi = 19/2^+$ isomers along the $N = 77$ chain, $J^\pi = 10^+$ states are characteristic isomers in $N = 78$ isotones. These isomers are interpreted as fully aligned $\nu h_{11/2}^{-2}$ configurations. The energy difference between $J^\pi = 10^+$ and the $J^\pi = 8^+$ states ranges from 18.5 keV in ^{130}Te to 378 keV in ^{142}Gd. The smooth evolution of the half-life with respect to the proton number is interrupted by a remarkable long half-life of $T_{1/2} = 8.39(11)$ ms [43] for the $J^\pi = 10^+$ isomer in ^{132}Xe, whereby the $J^\pi = 8_1^+$ state has not been observed to date [44]. Adding two protons, the half-life of the $J^\pi = 10^+$ state in ^{134}Ba was reported to be 2.63(14) μs [45]. In fact, the measured negative magnetic moment of this state ($\mu = -2.0(1)\ \mu_N$ [45,46]) strongly supports a $\nu h_{11/2}^{-2}$ configuration. The isomeric $J^\pi = 5^-$ state in ^{134}Ba at $E_x = 1986$ keV is subject of this publication. A previous half-life value was measured to be 52(6) ns following a ^{4}He + ^{133}Cs reaction by Ref. [21] and its longevity was attributed to a mixture of $\nu(s_{1/2}h_{11/2})$ and $\nu(d_{3/2}h_{11/2})$ configurations.

The low-spin structure of ^{134}Ba was studied in detail employing β decay [47], Coulomb excitation [48], and $(n, n'\gamma)$ reactions [49]. In contrast, information on the high-spin structure above the $J^\pi = 10^+$ ($T_{1/2} = 2.63(14)$ μs [45]) isomer is

tentative. The only evaluated data on high-spin states [50] refers to a preliminary level scheme from a JYFL (Accelerator Laboratory of the University of Jyväskyl) annual report by Lönnroth *et al.* [51] in 1990. In that study, two parallel cascades on top of the $J^\pi = 10^+$ isomer were identified using a ^{13}C + ^{124}Sn reaction inside the NORDBALL γ-ray spectrometer. Besides that result, two high-spin level schemes from works utilizing ^{14}C + ^{124}Sn and ^{9}Be + ^{130}Te reactions [52,53], respectively, differ significantly from each other as well as from evaluated data [50,51].

The scarce and contradictory experimental data in ^{133}Ba and ^{134}Ba together with recent theoretical advances motivate a refined investigation of high-spin features in both nuclei. In this article, we report and discuss new results on the high-spin regime of ^{133}Ba and ^{134}Ba. Excited states were populated in two complementary experiments using different reaction mechanisms. ^{134}Ba was populated in a ^{136}Xe + ^{208}Pb multinucleon-transfer experiment employing the high-resolution position-sensitive Advanced GAmma Tracking Array (AGATA) [54] in combination with the magnetic mass spectrometer PRISMA [55–57]. Furthermore, both ^{133}Ba and ^{134}Ba were investigated with a ^{13}C + ^{124}Sn fusion-evaporation experiment at the Institute of Nuclear Physics, University of Cologne. This paper is organized as follows: The experimental setup and data analysis of the two experiments are described in Sec. II, followed by the experimental results in Sec. III. A detailed comparison with shell-model calculations and systematics is presented in Sec. IV before the paper closes with a summary and conclusions in Sec. V.

II. EXPERIMENTAL PROCEDURE

A. ^{13}C + ^{124}Sn fusion-evaporation reaction

^{133}Ba and ^{134}Ba were populated simultaneously in a ^{13}C + ^{124}Sn fusion-evaporation reaction. The FN tandem accelerator of the Institute of Nuclear Physics, University of Cologne, delivered a 55-MeV ^{13}C beam impinging onto an enriched ^{124}Sn target with a thickness of 1.8 mg/cm^2 evaporated onto a 120-mg/cm^2-thick Bi backing plus a thick Cu layer for heat dissipation. The beam energy was optimized to populate mainly ^{133}Ba and ^{134}Ba via the (^{13}C, 4n) and (^{13}C, 3n) reaction channels, respectively. Both recoils and beam particles were stopped in the backing of the target. About 10^8 $\gamma\gamma$ coincidences were recorded. γ Rays were detected with a mixed γ-ray detector array employing eight high-purity germanium (hereafter called HPGe) and 12 cerium-doped lanthanum-bromide (hereafter called $LaBr_3$) detectors, mounted in the frame of the High efficiency Observatory for γ-Ray Unique Spectroscopy (HORUS) array [58]. Six of the $LaBr_3$ detectors were surrounded by bismuth-germanate (BGO) veto detectors to suppress the Compton background [59]. Coincident events were processed and recorded utilizing the synchronized 80-MHz XIA Digital Gamma Finder (DGF) data-acquisition system and stored to disk. The data were sorted offline using the SOCO-V2 [60] code and analyzed utilizing the ROOT [61] and TV [62] software packages.

Multipole-mixing ratios of transitions between excited states were investigated with the $\gamma\gamma$ angular-correlation code CORLEONE [63,64] based on the phase convention by Krane, Steffen, and Wheeler [65,66]. Different hypotheses of involved spins J_1, J_2, J_3 and multipole-mixing ratios δ_1, δ_2 of two coincident γ rays in a cascade $J_1 \xrightarrow{\delta_1} J_2 \xrightarrow{\delta_2} J_3$ were evaluated by χ^2 fits of the correlation function $W(\Theta_1, \Theta_2, \Phi) = W(J_1, \delta_1, J_2, \delta_2, J_3)$ to experimental intensities in six different correlation groups, each associated with detector pairs at angles $\Theta_{1,2}$ with respect to the beam axis and a relative angle Φ between the planes spanned by the detectors and the beam axis. More details on the angular-correlation analysis with CORLEONE are given in Refs. [67,68]

B. ^{136}Xe + ^{208}Pb multinucleon transfer

In a second experiment, ^{134}Ba was populated in a ^{136}Xe + ^{208}Pb multinucleon-transfer experiment at the Laboratori Nazionali di Legnaro, Italy. In this experiment, a 6.84-MeV/nucleon ^{136}Xe beam, accelerated by the PIAVE+ ALPI accelerator complex, impinged onto a 1-mg/cm^2 ^{208}Pb target. AGATA [54], in a first demonstrator configuration [69], was placed at a distance of 18.8 cm from the target position to measure γ rays from excited states. The array consisted of nine large-volume electronically segmented HPGe detectors in three triple cryostats [70]. An isotopic identification of the nuclei of interest was provided by the magnetic spectrometer PRISMA placed at the reaction's grazing angle of $\theta_{lab} = 42^\circ$. An event registered by the PRISMA focal-plane detector in coincidence with an AGATA event was taken as a trigger for the data acquisition. In this way, the origin of the γ rays is distinguished, background from β decay is reduced, and a major fraction of isomeric γ-ray transitions is suppressed.

Pulse-shape analysis of the digitized detector signals was applied to determine the individual interaction points within the HPGe detectors [71], enabling the Orsay forward-tracking algorithm [72] to reconstruct the individual emitted γ-ray energies and determine the first interaction point of the γ ray in the germanium and, thus, the emission angle. Together with the kinematic information from PRISMA, a precise Doppler correction was performed. Further details on the analysis can be found in Refs. [73,74].

III. EXPERIMENTAL RESULTS

A. ^{133}Ba

A partial level scheme of ^{133}Ba, including transitions of interest to this paper, is presented in Fig. 1(a). The determined half-lives of several isomeric states in ^{133}Ba and ^{134}Ba are summarized in Table I.

The 2366-keV ($J^\pi = 23/2^+$) state decays directly into the $J^\pi = 19/2^+$ isomer in ^{133}Ba. Figure 2(a) shows a E_γ-time matrix gated on the 424-keV ($23/2^+ \rightarrow 19/2^+$) transition. Coincidences between all eight HPGe detectors of the HORUS array were employed. The timestamps of the 424-keV transition were defined as reference time, and the maximum range for the correlation windows was chosen as 1.5 μs. Background contributions were subtracted by means of a similar matrix, gated on an area close to the 424-keV peak. Figure 2(b) presents the one-dimensional γ-ray spectrum time and energy gated on prompt events relative to

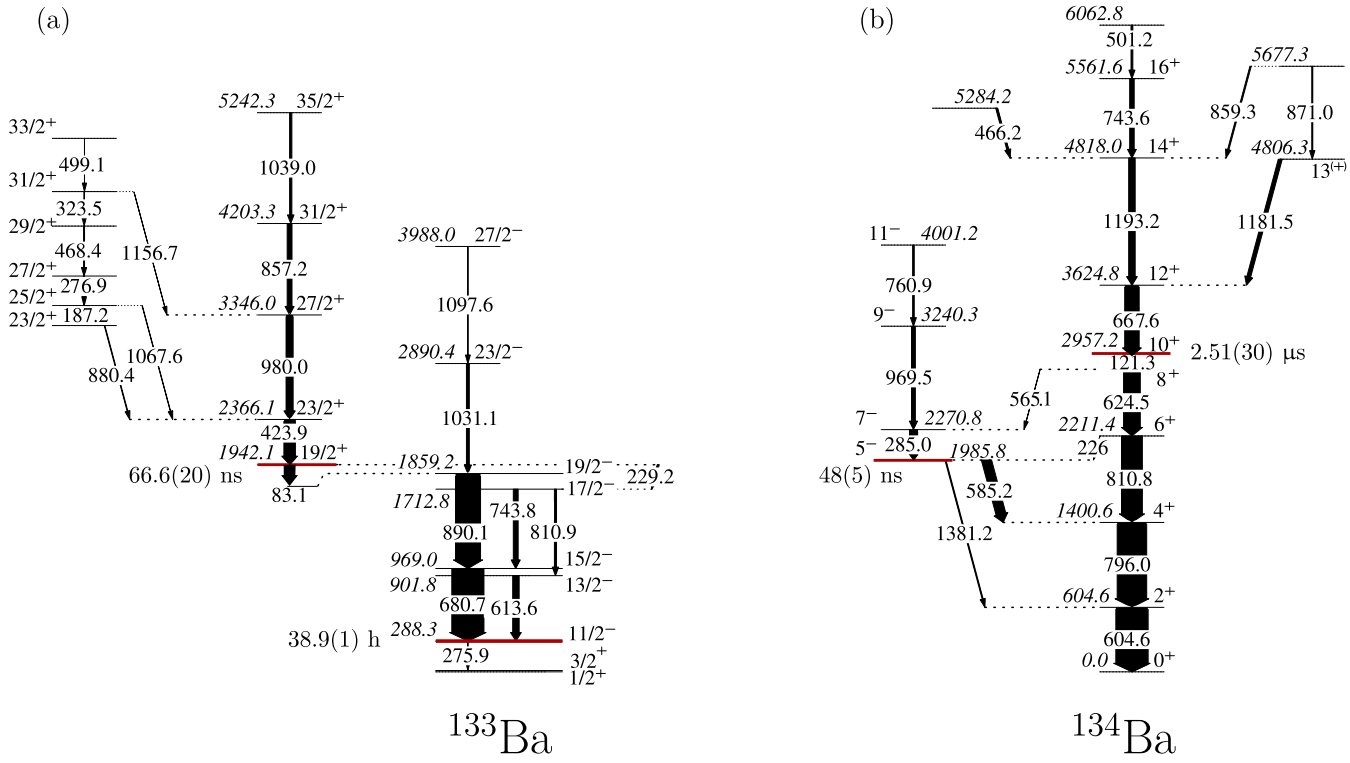

FIG. 1. (a) Partial level scheme of ^{133}Ba including transitions feeding or deexciting the 1942-keV state which is subject of this paper. Transitions and excitation energies are given in keV. Intensities, energies, and spins are adopted from Ref. [20]. For the $J^\pi = 19/2^+$ and $J^\pi = 11/2^-$ [50] states, the corresponding $T_{1/2}$ values are given in the figure. (b) Level scheme assigned to ^{134}Ba with the newly observed γ rays above the $T_{1/2} = 2.51(30)$ µs ($J^\pi = 10^+$) and $T_{1/2} = 48(5)$ ns ($J^\pi = 5^-$) isomers. Intensities are extracted from the HORUS data and normalized to the intensity of the 605-keV transition. The given half-lives of the $J^\pi = 19/2^+$ state in ^{133}Ba and of the $J^\pi = 5^-$ and 10^+ states in ^{134}Ba were newly determined.

the 424-keV transition as illustrated by the two-dimensional gate in Fig. 2(a). As expected, the feeding pattern of the 2366-keV state emerges in the spectrum up to the $J^\pi = 35/2^+$ state with strong transitions at 857, 980, and 1039 keV and less intensive transitions at 324, 468, 277, and 1068 keV. In addition, transitions below the isomer at 83, 229, 614, 681, 744, 810, and 890 keV are present, since the prompt area has a finite width.

For negative time differences, only random coincidences, e.g., e^-e^+ annihilation, are visible. Delayed transitions were obtained by gating on the positive time differences with respect to the 424-keV transition. Such a gate is visualized in the E_γ-time matrix shown in Fig. 2(c). The corresponding one-dimensional projection onto the energy axis is displayed in Fig. 2(d). The observation of members of γ-ray cascades deexciting the $J^\pi = 19/2^+$ state and the absence of the 1068-, 980- and, 857-keV feeding transitions confirm the presence of an isomer at $E_x = 1942$ keV in this nucleus. The half-life of the 1942-keV state has to be considerably longer than the proposed $T_{1/2} = 2$–5 ns [19], taking into account the measured time resolution of $\Delta t_{\mathrm{FWHM}} \approx 36$ ns.

TABLE I. Measured half-lives of selected isomers observed in the ^{13}C + ^{124}Sn experiment. The different columns indicate the nucleus, excitation energy, spin and parity of the isomeric state, the deduced weighted mean half-life, and previous results reported in the literature.

Isotope	E_x (keV)	J_i^π	$T_{1/2}$	
			Present work	Literature
^{133}Ba	1942	$19/2^+$	66.6(20) ns	2–5 ns [19]
^{134}Ba	2957	10^+	2.51(30) µs	2.63(14) µs [45]
^{134}Ba	1986	5^-	48(5) ns	52(6) ns [21]

In order to investigate the half-life of the $J^\pi = 19/2^+$ isomer, $\gamma\gamma$ matrices with various delayed coincidence time windows in the range between 3 (37.5 ns) and 20 ticks (250 ns) are generated. Coincidences between all eight HPGe detectors are taken into account. Subsequently, the intensities of the 681- and 890-keV γ-ray transitions (below the isomer) are determined in the $\gamma\gamma$ projection gated on the 424-keV transition (above the isomer). The direct decay of the $E_x =$ 1942-keV state at $E_\gamma = 83$ keV is partially contaminated by x rays of the ^{209}Bi backing which have very similar energies. Consequently, since the Weisskopf half-life estimates for $E_\gamma = 890$ and 681 keV is in the order of picoseconds and, therefore, considerably shorter than the half-life of the state of interest, an indirect gate is applied. The intensities N_t of the 681- and 890-keV γ-ray transitions, as a function of delayed coincidence time-window length, are fitted to Eq. (1):

$$N_t = N_0(1 - Ae^{-\frac{\ln(2)}{T_{1/2}}\Delta t}), \quad (1)$$

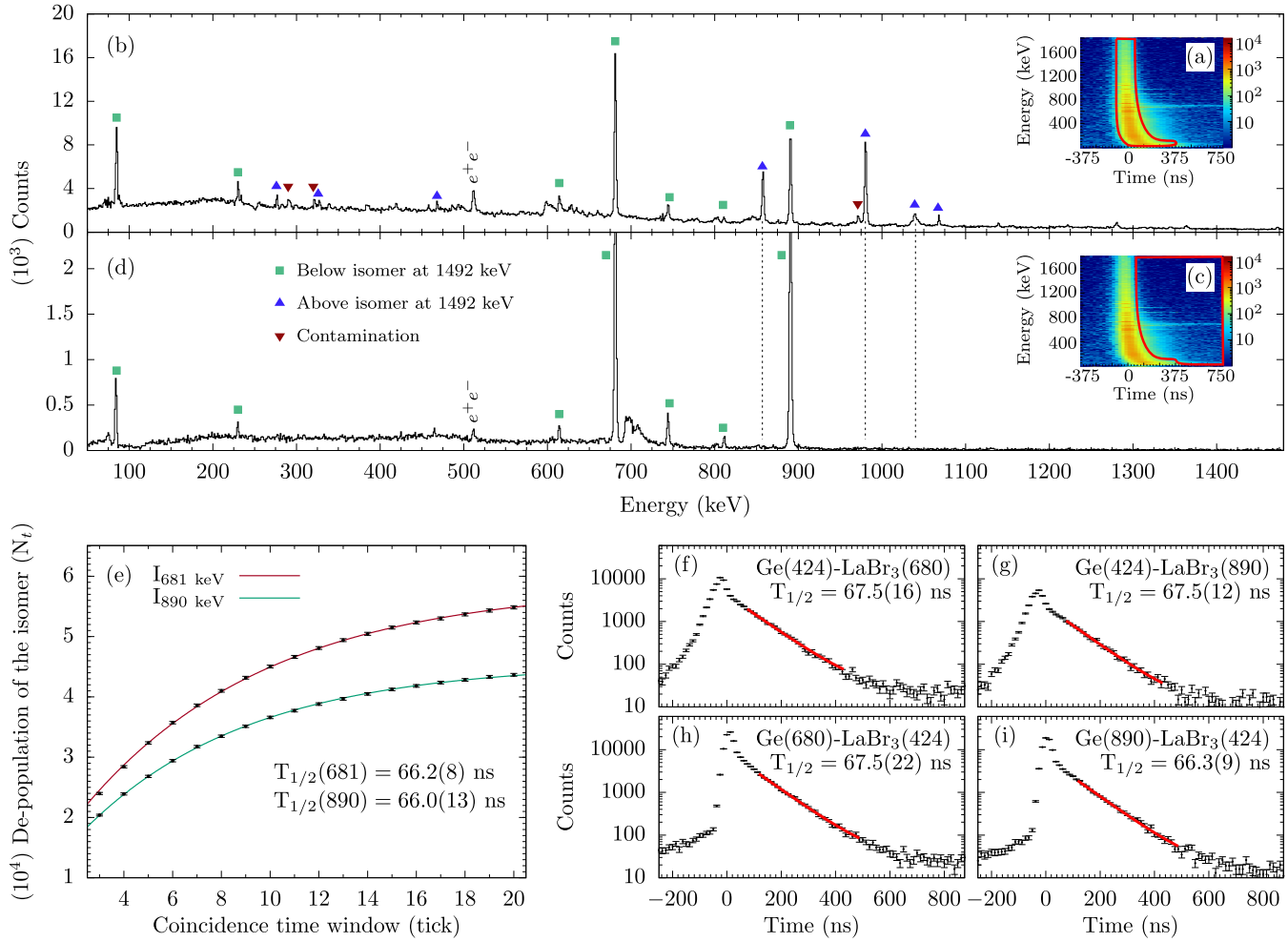

FIG. 2. [(a) and (c)] Two-dimensional E_γ-time matrices showing the time distribution of coincident γ-ray transitions relative to the 424-keV transition. The applied two-dimensional gates are surrounded by thick solid red lines. (b) Prompt and (d) delayed one-dimensional γ-ray spectra with respect to the 424-keV transition. (e) Plot of the fitted intensities of the 681- and 890-keV γ-ray transitions in the $\gamma\gamma$ projection gated on the 424-keV transitions as a function of coincidence time windows. The solid lines correspond to the fitted time distribution [see Eq. (1)]. One data acquisition time unit (tick) corresponds to 12.5 ns. [(f)–(i)] Gated E_γ-E_γ-time distributions and final lifetime fits for gating combinations between $LaBr_3$ and HPGe detectors. Half-lives are determined by exponential fits of the delayed component. The fit is drawn with a red solid line. The given half-lives include only the statistical uncertainties of the fits. For the total error see text.

where N_0, A, and the half-life $T_{1/2}$ are treated as free fitting parameters. Recently, this approach was successfully applied to isomers in the ns regime in ^{127}Xe [75]. Figure 2(e) presents the intensities of the 681- and 890-keV γ-ray transitions, gated on the 424-keV transition, with respect to the different coincidence time windows. The determined half-lives of $T_{1/2}(681\ \text{keV}) = 66.2(8)$ ns and $T_{1/2}(890\ \text{keV}) = 66.0(13)$ ns are in good agreement.

The combination of the excellent high-energy resolution of the HPGe detectors and the fast-timing capability of the $LaBr_3$ detectors is used to determine the half-life of the $E_x = 1942$-keV state independently from the aforementioned approach. A three-dimensional E_γ-E_γ-time cube is exploited, comprising energies of two γ rays respectively detected by a HPGe and a $LaBr_3$ detector and the corresponding timestamp difference between both events. Applying a narrow HPGe gate on the 424-, 680-, or 890-keV transitions, coincident γ-ray peaks are well separated from other lines in the $LaBr_3$ spectrum allowing clear gate conditions. Figures 2(f)–2(i) show several spectra of time differences between HPGe and $LaBr_3$ events. In the time spectra shown in Figs. 2(f) and 2(g), the feeding 424-keV γ ray is detected by HPGe detectors and the decaying 680- and 890-keV transitions are detected by $LaBr_3$ detectors. In contrast, in Figs. 2(h) and 2(i) the 424-keV feeding transition is detected by $LaBr_3$ detectors, while the decaying 680- and 890-keV transitions are detected by HPGe detectors. Using the $LaBr_3$ detectors as start detectors, the prompt curve is sharper, as illustrated by comparing Figs. 2(f) and 2(g) with Figs. 2(h) and 2(i). The short-lived component in the prompt peak is mainly caused by Compton background. Half-lives are extracted by fitting a function of the form $N(t) = a\exp[t\ln(2)/T_{1/2})] + b$ to the tail of the time distributions. The parameter b is determined from the background and kept constant. Exponential fits of the long-lived slope component yield half-life values of 67.5(16), 67.5(12), 67.5(22), and 66.3(9) ns, visualized with a red solid line in Figs. 2(f)–2(i).

TABLE II. Energies, spin assignments, and relative in-beam intensities for new γ-ray transitions in ^{134}Ba above the $J^\pi = 10^+$ isomer at $E_x = 2957$ keV. Fitted energies and relative intensities normalized to the 668-keV transition are taken from two experiments: I_γ^1 from the HORUS ^{13}C + ^{124}Sn reaction and I_γ^2 from the AGATA ^{136}Xe + ^{208}Pb experiment.

E_γ (keV)	E_i (keV)	E_f (keV)	I_i^π	I_f^π	I_γ^1	I_γ^2
466.2	5284.2	4818.0	–	14^+	16(3)	23(3)
501.2	6062.8	5561.6	–	16^+	14(2)	–
667.6	3624.8	2957.2	12^+	10^+	$\equiv 100$	$\equiv 100$
743.6	5561.6	4818.0	16^+	14^+	30(4)	20(2)
859.3	5677.3	4818.0	–	14^+	Weak	–
871.0	5677.3	4806.2	–	$13^{(+)}$	Weak	–
1181.5	4806.3	3624.8	$13^{(+)}$	12^+	38(4)	–
1193.2	4818.0	3624.8	14^+	12^+	50(5)	62(9)

Moreover, the independently determined values from Fig. 2(e) are in good agreement, showing the complementarity between both approaches. Systematic errors from background contributions at the borders of the fit interval as well as uncertainties in the determination of the background parameter are conservatively taken into account. The weighted mean half-life value over the six independent values results in $T_{1/2} = 66.6 \pm 0.5$ (stat.) ± 1.9 (syst.) ns for the 1942-keV state in ^{133}Ba. This corresponds to a $B(E1; 19/2^+ \rightarrow 19/2^-)$ value of $7.7(4) \times 10^{-6}$ e^2 fm^2 using relative γ-ray intensities of 100(12)% and 9(1)% for the 83- and 229-keV transitions, respectively.

B. ^{134}Ba

The extended level scheme of ^{134}Ba achieved in the present work is displayed in Fig. 1(b). Measured intensities of coincident γ rays above the $J^\pi = 10^+$ isomer in ^{134}Ba obtained from the HORUS and AGATA experiments are summarized in Table II. Intensities are from the HORUS ^{13}C + ^{124}Sn reaction (I_γ^1) as well as from the AGATA ^{136}Xe + ^{208}Pb experiment (I_γ^2). The independently measured intensities show a consistent assignment of states and transitions. The uncertainties in the transition energies are ± 0.5 keV. Spin-parity assignments are supported by angular-correlation measurements, shell-model calculations, and systematics.

The beam-like Doppler-corrected singles γ-ray spectra of ^{134}Ba from the ^{136}Xe + ^{208}Pb AGATA experiment is shown in Fig. 3(a). The corresponding Ba mass distributions is depicted in the inset Fig. 3(b). Random background is significantly suppressed by gating on the prompt peak in the time-difference distribution between AGATA and PRISMA. The full width at half-maximum (FWHM) of the prompt coincidence peak is about 16 ns for identified beamlike particles. Due to the presence of two long-lived $J^\pi = 10_1^+$ and $J^\pi = 5_1^-$ isomers in the level scheme of ^{134}Ba, transitions of the yrast $10^+ \rightarrow 8^+ \rightarrow 6^+ \rightarrow 4^+ \rightarrow 2^+ \rightarrow 0^+$ cascade and the $5^- \rightarrow 4^+$ transition are suppressed in the spectrum. None of the known low-spin excited yrare states below 3 MeV [49] were populated. As reported in Ref. [51], we identify the 285-, 761-, and 970-keV γ rays to be transitions of the negative-parity band of ^{134}Ba. The measured relative intensities of the three γ rays support the known ordering of the γ rays within the negative-parity band. New peaks well above the background level are observed at energies of 171, 178, 466, 668, 744, and 1193 keV. As the negative-parity band is completely identified, it is most likely that the new transitions are members of cascades feeding the $J^\pi = 10^+$ isomer. The existence of 681–914–800-keV and 1131–547-keV cascades feeding the $J^\pi = 10^+$ isomer suggested by Lönnroth *et al.* [51] could not be confirmed. Transitions at energies of 171 and 178 keV could not be assigned using the HORUS data, as discussed below.

^{134}Ba was also populated in the ^{13}C + ^{124}Sn fusion-evaporation reaction. Figure 4(a) shows a background-subtracted E_γ-time matrix, gated on the delayed $2^+ \rightarrow 0^+$ 605-keV transition. Transitions feeding the $J^\pi = 10^+$ isomer are visible at negative time differences in this matrix representation. Time distributions following an exponential decay curve are visible at energies of 668 and 1193 keV. The

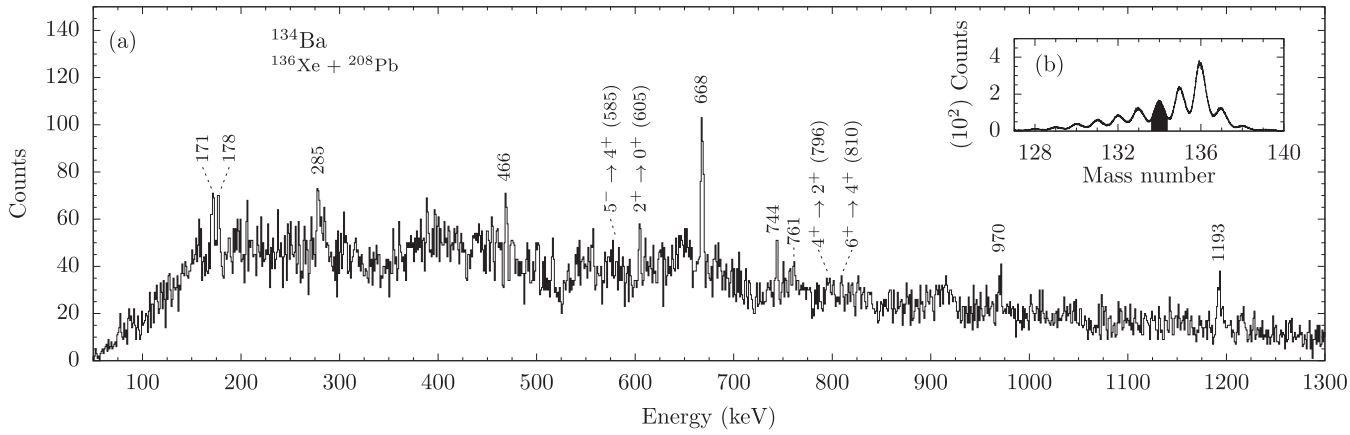

FIG. 3. (a) Doppler-corrected γ-ray spectrum gated on ^{134}Ba identified with PRISMA in the ^{136}Xe + ^{208}Pb experiment. Random background is reduced with a gate on the prompt peak in the spectrum of time differences between AGATA and PRISMA. Inset (b) represents the mass spectrum of the Ba isotopes obtained with PRISMA. The applied mass gate on ^{134}Ba is marked black.

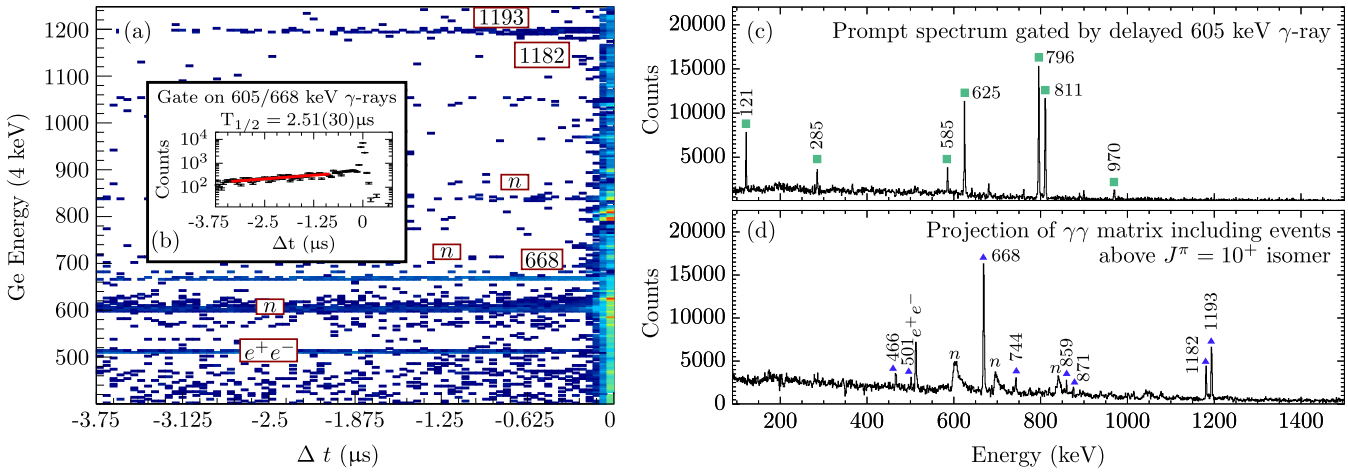

FIG. 4. Results of the HORUS experiment showing (a) E_γ-time matrix with respect to the $2^+ \rightarrow 0^+$ 605-keV transition. (b) Time difference spectrum between the 668- and 605-keV transitions, extracted from the E_γ-time matrix. (c) One-dimensional HORUS γ-ray spectrum gated on the 605-keV transition. Transitions below the $J^\pi = 10^+$ isomer are predominantly visible. (d) Projection of a HORUS $\gamma\gamma$ matrix sorted by gating on negative timestamp differences relative to the timestamp of the delayed ground-state band of ^{134}Ba with 605-, 796-, 810-, 625- or 121-keV transitions. Only transitions above the $J^\pi = 10^+$ isomer are visible. Ge$(n, n\gamma)$ edges are marked with n. See text for details.

isomer half-life is deduced from the analysis of timestamp differences between the 668- and 605-keV transitions, obtained by projecting the time distribution of the 668-keV transition onto the x axis in Fig. 4(a). The time spectrum and an exponential fit is shown in the inset in Fig. 4(b). The determined half-life of $T_{1/2} = 2.51(30)$ μs is in excellent agreement with the evaluated half-life value for the $J^\pi = 10^+$ state by Bell *et al.* [45]. Consequently, in accordance with the observation in the AGATA experiment shown in Fig. 3(a), the 668-keV transition is unambiguously assigned to a state above the $J^\pi = 10^+$ isomer in ^{134}Ba.

Transitions below the long-lived $J^\pi = 10^+$ isomer were identified by a time- and energy-gated one-dimensional γ-ray spectrum exhibiting coincidences within the prompt time peak relative to the delayed 605-keV transition. The corresponding spectrum is shown in Fig. 4(c). The positive-parity $E2$ ground-state band is visible up to the $10^+ \rightarrow 8^+$ 121-keV decay. To assign the new transitions to the known level scheme of ^{134}Ba, events were further sorted into a three-dimensional $\gamma\gamma\gamma$-cube, whereby one γ ray corresponds to a transition in the $E2$ ground-state band up to the $J^\pi = 10^+$ isomer (605, 796, 810, 625, or 121 keV). Thereafter, events were further processed into a prompt two-dimensional $\gamma\gamma$ matrix including double coincidences (within 100 ns) which meet the condition of negative timestamp differences in the range between −3.75 μs and −0.3 μs from the reference timestamps of the delayed 605-, 796-, 810-, 625-, or 121-keV transitions. The requirement ensure that the $\gamma\gamma$ matrix exhibits only transitions above the $J^\pi = 10^+$ isomer. Figure 4(d) shows the γ-ray projection of this matrix. The spectrum is dominated by transitions at 466, 668, 744, 1182, and 1193 keV. The intensity balance in both the AGATA [Fig. 3(a)] and HORUS [Fig. 4(d)] experiments require the newly observed 668-keV transition to be placed directly above the $J^\pi = 10^+$ isomer, deexciting a new state at 3625-keV excitation energy. Various $\gamma\gamma$-coincidence spectra from this matrix are shown in Figs. 5(a)–5(d). Figure 5(a) presents the γ-ray spectrum with a gate on 668 keV. The spectrum exhibits anticipated coincidence peaks at 466, 501, 744, 859, 871, 1182, and 1193 keV. The 668-keV transition is in mutual coincidence with the 1193-, 744-, and 501-keV transitions [Figs. 5(b) and 5(c)]. Thus, all three γ rays form a cascade on top of the 3625-keV state. By gating on the 668-keV transition, the intensity balance requires that the 1193-keV transition is placed on top of the 668-keV transition. Moreover, the ordering of the 744-, and the 501-keV transitions above the newly established $E_x = 4818$ keV state agrees with the intensity balance of the $\gamma\gamma$ projections gated on the 668- and 1193-keV transitions. Other peaks at 466, 859, 871, and 1182 keV are observed to be in coincident with the 668-keV transition [Fig. 5(a)]. Moreover, the 871- and 1182-keV lines are in mutual coincidence depopulating two states at $E_x = 5677$ and 4806 keV. The absence of the 871–1182-keV cascade and the occurrence of the 859-keV peak in Fig. 5(b) requires the 859-keV transition to be placed parallel to this cascade. Additionally, the 871–1182-keV cascade corresponds to the sum energy of the 1193–859-keV cascade, supporting the assignment. A 466-keV transition is in coincidence with the 1193–668-keV cascade [Figs. 5(a) and 5(b)] but not with the 744-keV transition. Consequently, the 466-keV γ ray is placed on top of the 4818-keV state.

Going to the negative-parity band, Fig. 5(d) shows a γ-ray spectrum for ^{134}Ba obtained by gating on the $5^- \rightarrow 4^+$ 585-keV transition. The spectrum demonstrates that the 761–970–285-keV cascade is placed on top of the $J^\pi = 5^-$ isomer. The inset Fig. 5(d) visualizes the time spectrum between the 761–970–285-keV and the 585–796–605-keV cascades. An exponential fit yields a half-life of 48(5) ns, which is in good agreement with the previous value of 52(6) ns [21].

Spin assignments can be tested in the HORUS experiment with the procedure discussed in Sec. II A. Figure 6(a) shows a benchmark angular-correlation fit of the experimentally deduced relative intensity distribution (data points) with a theoretical angular-correlation function (line) of the $4^+ \rightarrow 2^+$

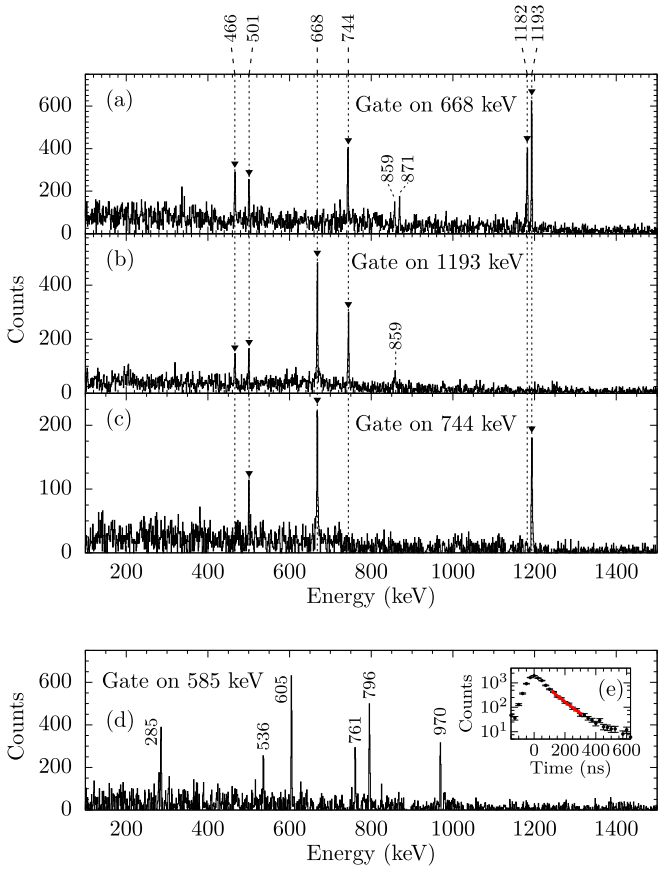

FIG. 5. γ-Ray spectra above the $J^\pi = 10^+$ isomer, gated on (a) 668, (b) 1193, and (c) 744 keV. (d) $\gamma\gamma$-coincidence spectra with a gate on the $5^- \rightarrow 4^+$ 585-keV transition. (e) Time spectrum between the 761–970–285-keV (prompt) and 585–796–605-keV (delayed) cascades with an exponential decay-curve fit (red solid line). The fitted half-life is 48(5) ns.

796-keV decay in ^{134}Ba, gated on the 605-keV transition. Fixing the multipole-mixing ratio of the 605-keV transition to quadrupole character ($\delta_1 = 0$) and varying the δ_2 value yields a χ^2 minimum of 1.1. The obtained multipole-mixing ratio of $\delta_2 = 0.02(3)$ is in agreement with the expected quadrupole character.

Based on the known $J^\pi = 10^+$ spin of the 2957-keV state, the spins of the newly established 3625- and 4818-keV states in ^{134}Ba are evaluated. Scenarios of $J_1 = \{10, 11, 12\} \rightarrow \delta_1 J_2 = 10 \xrightarrow{\delta}{}_2 =$ fixed$J_3 = 10$ and $J_1 = \{11, 12, 13\} \xrightarrow{\delta_1} J_2 = 11 \xrightarrow{\delta_2=\text{fixed}} J_3 = 10$ were tested for the 1193–668-keV cascade. Fits with several fixed multipole-mixing ratios of the 668-keV transitions ($\delta_2 = 0,\ \pm 0.05,\ \pm 0.1,\ \pm 0.15, \ldots$) yields χ^2 values of larger then 2.3. In contrast, the $J_1 = 14 \xrightarrow{\delta_1} J_2 = 12 \xrightarrow{\delta_2=0} J_3 = 10$ hypothesis with fitted $\delta_1 = -0.01(3)$ value for the 1193-keV transition yields the best χ^2 value of 1.3, as shown in Fig. 6(b). Apart from that, similar fits assuming a nonzero δ_2 value for the 668-keV transition yield significantly worse χ^2 values. Hence, the best agreement is obtained for a pure-quadrupole $J_1 = 14 \rightarrow J_2 = 12 \rightarrow J_3 = 10$ cascade. Since a $M2$ multipolarity in this cascade would cause long-lived states and other isomers, a positive parity is assigned to the 3625- and 4818-keV states. Employing the same method, the spin of the newly established excited state at 5562 keV is determined. The 744–1193-keV cascade is best reproduced assuming a spin of $J = 16$ for the 5562-keV state ($\chi^2 = 1.4$). In accordance with the fitted $\delta_1 = 0.01(2)$ value, a positive parity is assigned for the 5562-keV state. In contrast, the 1182-keV transition yields a dipole character with multipole-mixing ratio of $\delta_1 = -0.06(4)$. Consequently, the spin-parity of the 4806-keV state is interpreted as $J = 13^{(+)}$.

The bandhead of the negative-parity band at $E_x = 1986$ keV and the first excited state above the bandhead at $E_x = 2271$ keV were identified as $J^\pi = 5^-$ and $J^\pi = 7^-$ states by Lönnroth *et al.* [51]. However, spin-parity assignments of states on top of the bandbead with excitation energies of 3240 and 4001 keV were tentative in the previous work. Similarly to the aforementioned discussion, Fig. 6(c) shows the experimentally deduced angular-correlation intensity distribution for the coincident γ rays at 285 and 970 keV, compared to calculated values for different scenarios with spin values of $J = 7$, 8, and 9 for the 3240-keV state. A hypothesis of $J = 9$ for the 3240-keV state yields the best result. The vanishing multipole-mixing ratio of $\delta_1 = 0.00(2)$ indicates a negative parity of the 3240-keV state. Going to higher states in the band, angular-correlation fits with spin assignments of $J = 9$ and 10 for the 4001-keV state yield only limited agreement with the data. Instead, a good match is obtained by assuming

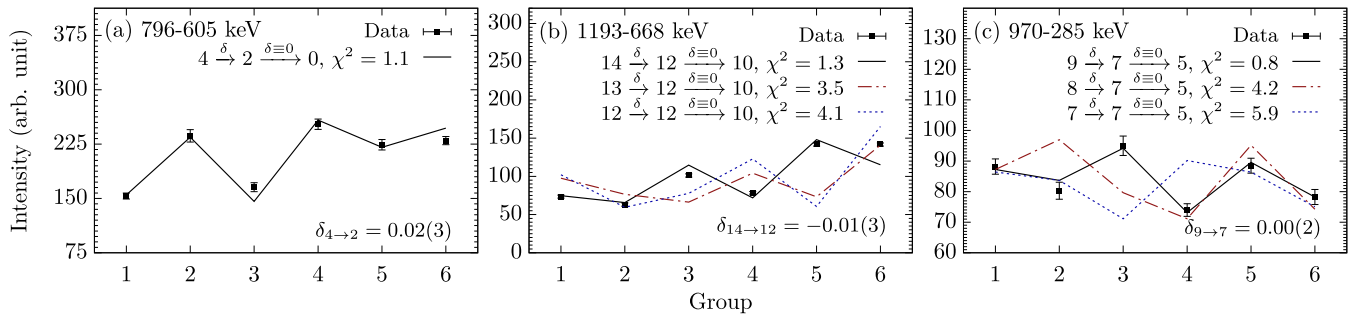

FIG. 6. (a) Benchmark $\gamma\gamma$ angular correlations for the $4^+ \rightarrow 2^+ \rightarrow 0^+$ (796–605-keV) cascade in ^{134}Ba. Experimental values (data points) are compared to calculated angular-correlation functions $W(\Theta_1, \Theta_2, \Phi)$ (lines) for six correlation groups using the code CORLEONE [63,64]. Investigation for (b) the newly established 668-1193-keV cascade and (c) the 285–970-keV cascade in ^{134}Ba.

a $J = 11$ state with dominant quadrupole ($E2$) character [$\delta_1 = 0.02(3)$]. The results are given in Fig. 1(b).

IV. SHELL-MODEL CALCULATIONS AND DISCUSSION

The obtained lifetime of the $19/2^+$ state in ^{133}Ba and the extended high-spin level schemes of ^{134}Ba are discussed and compared with the results of shell-model calculations and systematics. Five shell-model calculations were carried out in an untruncated $50 \leqslant Z, N \leqslant 82$ $gdsh$ valence space. The single-particle space is generated by the valence nucleons occupying the $0g_{7/2}$, $1d_{5/2}$, $1d_{3/2}$, $2s_{1/2}$, and $0h_{11/2}$ orbitals, outside doubly magic ^{100}Sn. In a further calculation using the EPQQM interaction, the $gdsh$ valence space is extended by the $1f_{7/2}$ neutron orbit above the $N = 82$ shell closure to calculate the $E1$ transition strength value of the $19/2^+ \rightarrow 19/2^-$ transition in ^{133}Ba. Shell-model calculations were carried out employing the shell-model code NuShellX@Msu [76], the massive-parallelization code KSHELL [77], and the ANTOINE shell-model code [78].

The first calculation is conducted with the effective interaction GCN50:82 [1,2]. The interaction is derived from a realistic G matrix based on the Bonn-C potential [79]. Empirical monopole corrections to the original G matrix are introduced by fitting different combinations of two-body matrix elements to sets of experimental excitation energies from even-even and even-odd semimagic nuclei.

The second calculation is carried out with the jj55pn Hamiltonian (referred to as the SN100PN interaction) [3]. The Hamiltonian consists of four terms describing the neutron-neutron, neutron-proton, proton-proton, and Coulomb repulsion between the protons individually. A renormalized G matrix derived from the CD-Bonn interaction [79] was employed to construct the realistic two-body residual interaction. The proton and neutron single-particle energies are based on the energy levels in ^{133}Sb and ^{131}Sn.

Another calculation is conducted with the SNV interaction [4]. The interaction combines the proton-proton N82GYM interaction [80] with the semiempirical SNBG3 neutron-neutron interaction [81] and the monopole-based universal ($V_{\rm MU}$) interaction for the proton-neutron part [82,83]. Both the SNBG3 and N82GYM interactions are G-matrix-based interactions. The SNBG3 interaction is obtained by combining the next-to-next-to-next-to-leading order interaction with a χ^2 fit of levels including 3^-_1 states along ($N < 82$) Sn isotopes. Strengths of the central and the tensor force from the orginal $V_{\rm MU}$ interaction are multiplied by 0.84 and 1.3, respectively, to fit the experimental data of one-proton separation energies in Sb isotopes [84]. Very recently, the interaction successfully described the g factor of the $J^\pi = 23/2^+$ state in ^{135}La [4].

A fourth calculation is performed utilizing the framework of the pair-truncated shell model, denoted as PQM130 (pairing+QQ+ multipole for mass region 130). The approach leverages a pairing-plus-quadrupole interaction that consists of spherical single-particle energies, a monopole-pairing, a quadrupole-pairing, and a quadrupole-quadrupole interaction. The Hamiltonian in each neutron and proton space is diagonalized separately and afterward the total Hamiltonian is diagonalized in the truncated space. More details on the calculation are given in Refs. [5,6].

A fifth calculation is performed in the framework of the realistic shell model [7,8], denoted as Realistic SM. Single-particle energies and two-body effective interaction are determined from the established CD-Bonn free nucleon-nucleon potential [79] using the $V_{\text{low-}k}$ approach with a cutoff momentum of $\Lambda = 2.6$ fm^{-1}, plus the Coulomb force for protons. The effective shell-model Hamiltonian is derived iteratively by means of the many-body perturbation theory in the $\hat{Q}$-box folded diagram expansion, including all diagrams up to third order in the interaction. More details can be found in Ref. [85].

The last calculation is conducted in the framework of the extended pairing plus quadrupole-quadrupole force with monopole corrections model (EPQQM) [86–89]. Single-particle energies (SPEs) were adopted from the experimental excited states of ^{133}Sb (proton SPEs) and ^{131}Sn (neutron SPEs). The $gdsh$ valence space is enlarged by the $\nu 1f_{7/2}$ neutron orbit above the $N = 82$ shell closure. Calculations within this large valence space allow us to describe $E1$ transitions. The interaction was recently successfully applied to neutron-rich nuclei around ^{132}Sn [9,90–93].

A. ^{134}Ba

A comparison of the experimentally obtained energy spectrum of ^{134}Ba with the results of the shell-model calculations is presented in Fig. 7. Moreover, yrare $J^\pi = 2^+_2$, 4^+_2, and 8^+_2 states from the literature are compared as further benchmarks for the validity of the shell-model calculations. All calculations reproduce the hitherto known members of the positive-parity ground-state band up to the $J^\pi = 10^+$ isomer quite well. In particular, the excitation energy of the $J^\pi = 10^+$ isomer is predicted at 2.953 (GCN50:82), 2.517 (SN100PN), 2.911 (SNV), 2.915 (PQM130), and 3.010 MeV (Realistic SM) which are in good agreement with the experimentally determined 2.957 MeV. The small 121-keV energy gap between the $J^\pi = 8^+$ and the 10^+ states is reasonably reproduced by the calculated energy gaps of 10 and 60 keV in the GCN50:82 and PQM130 interactions, respectively. However, the order of $J^\pi = 10^+$ and 8^+ states is interchanged in the SN100PN, SNV, and Realistic SM calculations.

In Sec. III B a $16^+ \rightarrow 14^+ \rightarrow 12^+ \rightarrow 10^+$ cascade with γ-ray energies of 744, 1193, and 668 keV was newly established. This assignment is supported by calculated transition energies of 672, 1327, and 609 keV (GCN50:82), 674, 1016, and 765 keV (SNV), 744, 1215, and 675 keV (PQM130), and 893, 997, and 732 keV (Realistic SM) for this cascade. Although the excitation spectrum calculated by SN100PN is more compressed, the relative position of the $J^\pi = 16^+$, 14^+, 12^+, and 10^+ states are in good agreement with the experimental excitation spectrum.

The 5677-keV state decays partially via a one-step decay into the $J^\pi = 14^+$ state and via a two-step cascade through the $J^\pi = 13^{(+)}$ state into the $J^\pi = 12^+$ state. Consequently, this state is interpreted to have a spin of $J = 14$ or 15. The yrast $J^\pi = 15^+$ state is predicted at 376 (GCN50:82), 352 (SNV), 478 (SN100PN), and 514 keV (PQM130) above the $J^\pi = 14^+_1$ state, which contradicts the observed 859-keV

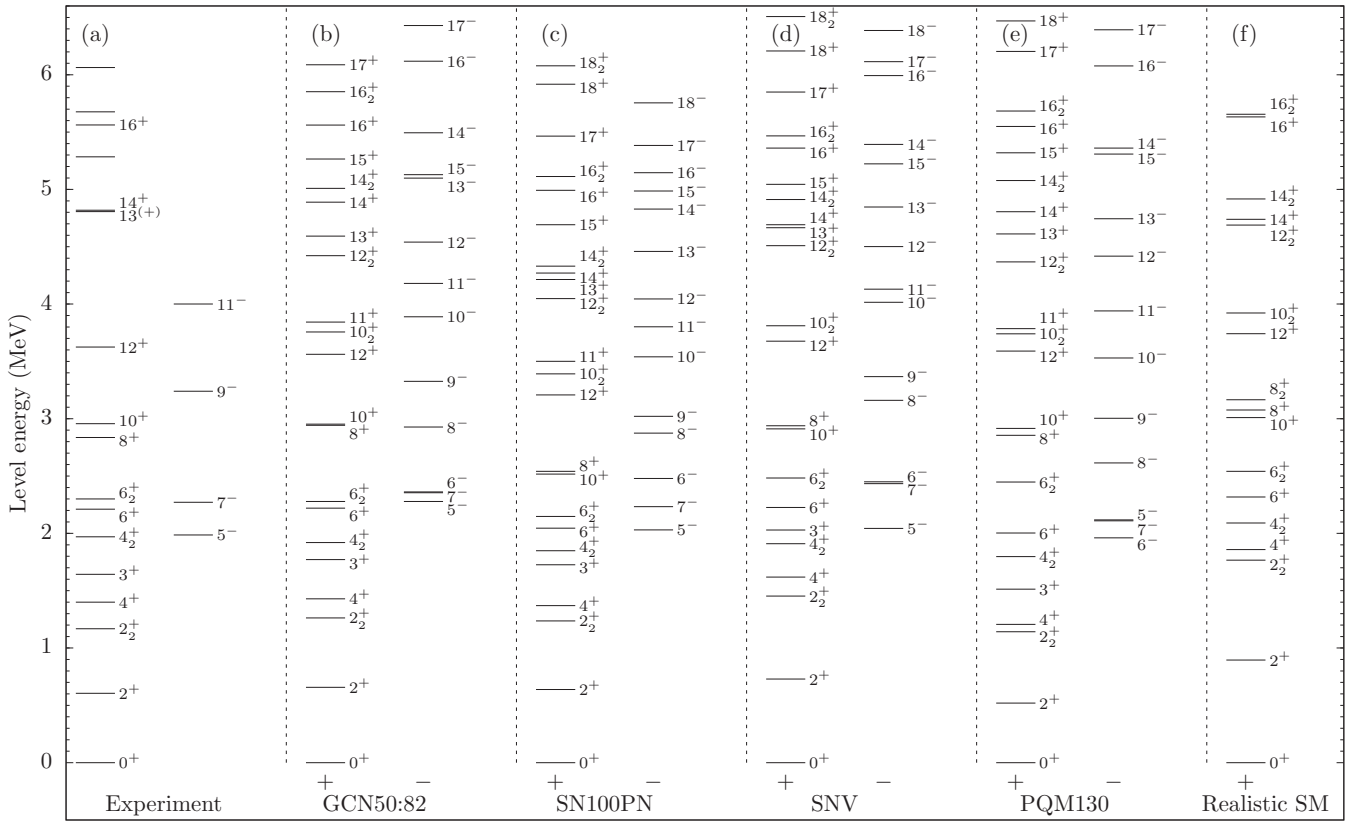

FIG. 7. Comparison of experimental energy spectra with the results of shell-model calculations for ^{134}Ba. (a) Experimental energy spectrum. The results obtained with the different interactions are separated in different columns: (b) GCN50:82, (c) SN100PN, (d) SNV, (e) PQM130, and (f) Realistic SM. For clarity, the states are separated into columns for the negative- and the positive-parity states.

energy difference between the $E_x = 5677$ keV and the $J^\pi = 14^+$ state. Similarly, a possible $J^\pi = 14^+_2$ state is predicted slightly above the $J^\pi = 14^+_1$ state. Consequently, a positive parity for the state at $E_x = 5677$ keV is unlikely. A better agreement of a $J^\pi = 14^+_2$ or 15^+_1 assignment is achieved for the 5284-keV state which is only 466 keV above the $J^\pi = 14^+_1$ state. However, no conclusive assignment can be made, since the calculated level density of states is too high.

Going to the negative-parity band, the calculations tend to slightly overpredict the excitation energy of the $J^\pi = 5^-$ bandhead. GCN50:82 predict the state at 2278 keV, SN100PN at 2030 keV, SNV at 2043 keV, and PQM130 at 2118 keV compared to the experimental 1986-keV excitation energy. A good agreement is obtained for the position of the calculated $J^\pi = 7^-$ state which deviates only 84 (GCN50:82), 37 (SN100PN), 163 (SNV), and 161 keV (PQM) from the experimental excitation energy. On the other hand, $J^\pi = 5^-$, 6^-, and 7^- states are permuted in the PQM130 calculation. All shell-model calculations consistently support a large energy gap of 972 (GCN50:82), 788 (SN100PN), 933 (SNV), and 895 keV (PQM130) between the $J^\pi = 9^-$ and $J^\pi = 7^-$ states, which agrees well with the observed 970 keV. The $J^\pi = 11^-$ state is calculated to be 763–935 keV higher in excitation energy with respect to the $J^\pi = 9^-$ state, supporting an $J^\pi = 11^-$ assignment for the $E_x = 4001$-keV state.

Moreover, the shell-model results provide insight into the structure of the isomeric states and the new established levels in ^{134}Ba. States below the $J^\pi = 10^+$ isomer are dominated by proton spin contributions. For example, the total spin of the $J^\pi = 8^+$ state is attributed to 26% $\nu_{2^+} \otimes \pi_{6^+}$ and 20% $\nu_{0^+} \otimes \pi_{8^+}$ with a leading configuration of $\nu(d^{-2}_{3/2}h^{-2}_{11/2}) \otimes \pi(g^4_{7/2}d^2_{5/2})$, using GCN50:82. On the other hand, a predominant neutron character takes over from the $J^\pi = 10^+$ state onward. The $J^\pi = 10^+$ isomer is calculated to be of $(\nu h^{-2}_{11/2})$ character with a spin configuration of 39% $\nu_{10^+} \otimes \pi_{0^+}$ and 32% $\nu_{10^+} \otimes \pi_{2^+}$. Likewise, the yrast states $J^\pi = 12^+$, 14^+, and 16^+ consist of a neutron ν_{10^+} configuration coupled to even-spin proton configurations. According to the GCN50:82 calculation, the leading configurations of the $J^\pi = 5^-$ isomer are (3%) $\nu(d^{-1}_{3/2}h^{-1}_{11/2})$ and (10%) $\nu(s^{-1}_{1/2}h^{-1}_{11/2})$. The calculation describes the negative-parity states above the $J^\pi = 5^-$ isomer with a neutron angular momentum of $7\hbar$ coupled to the proton quadrupole excited states (0^+, 2^+, 4^+).

Figures 8(a) and 8(b) show the evolution of several states in the positive- and negative-parity yrast band along the $N = 78$ isotones ranging from ^{130}Te to ^{142}Gd. The newly established states of ^{134}Ba are marked with thicker lines. The $16^+ \rightarrow 14^+ \rightarrow 12^+ \rightarrow 10^+$ cascade in ^{134}Ba fits the systematics [Fig. 8(a)]. Moreover, the reevaluated negative-parity band is in good agreement with the systematics [Fig. 8(b)]. Similarly to the $N = 78$ chain, Fig. 8(c) presents the evolution of positive-parity excited states along the Ba isotopes. The mid-shell Ba nuclei exhibit excitation spectra which are rotational in character, while a gradual change to a vibrational character

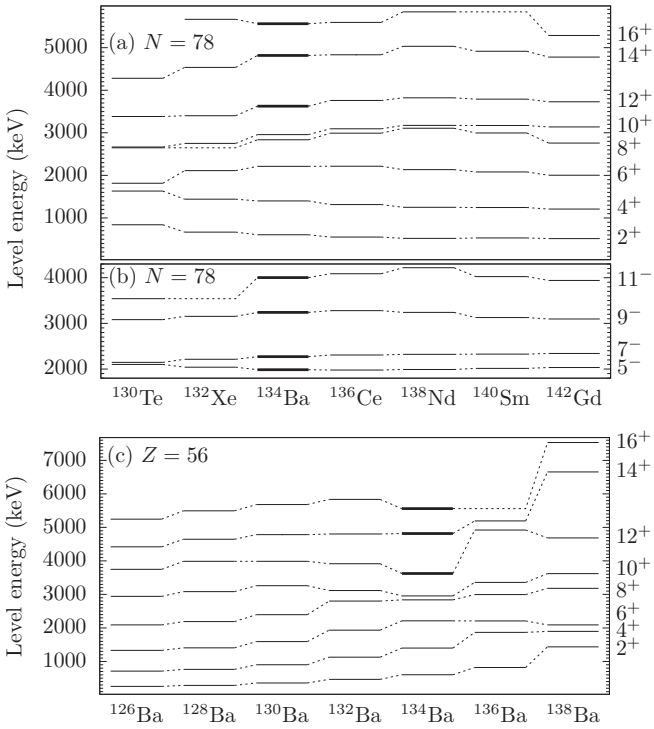

FIG. 8. Evolution of excited states along the even-mass $N = 78$ isotones for (a) the positive-parity yrast states and (b) for the negative-parity yrast states. (c) Evolution of positive-parity yrast states along the $Z = 56$ even-mass Ba isotopes. Newly discovered states in ^{134}Ba are marked with thick lines. Data taken from Refs. [50, 94–96].

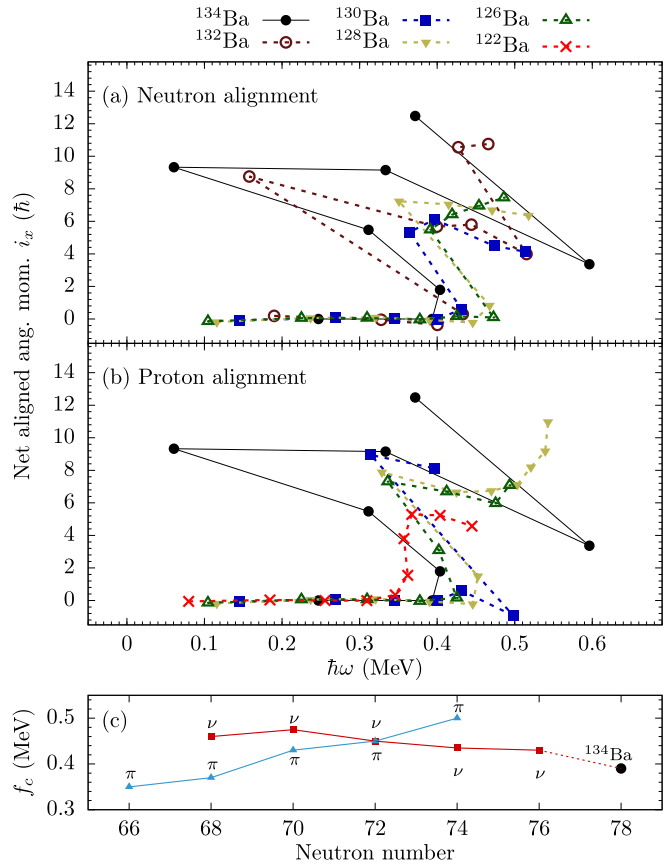

FIG. 9. Evolution of net aligned angular momenta $i_x(\hbar)$ along the even-mass Ba chain as a function of rotational frequency $\hbar\omega$. Isotopes along the Ba chain exhibit two S bands with (a) neutron-hole ($\nu h_{11/2}^{-2}$) and (b) proton ($\pi h_{11/2}^{2}$) configurations. (c) Summary of observed crossing frequencies between ground-state band and S bands based on proton (π) and neutron (ν) configurations for Ba isotops. The frequencies have been determined from net aligned angular momenta plots. Data extracted from Refs. [50,96].

is observed when approaching the $N = 82$ shell closure. ^{134}Ba lies in between, demonstrating the transitional character of this nucleus.

Backbending and upbending phenomena in the positive-parity yrast bands of even-even Ba isotopes were systematically investigated in the past. A comparison of the net aligned angular momentum $i_x(\omega)$ of the positive-parity band in ^{134}Ba with the corresponding bands in lower even-mass neighbors $^{132-126}$Ba and ^{122}Ba is displayed in Figs. 9(a) and 9(b). The ground-state cascade below the crossing serve as reference and is fitted according to Harris *et al.* [97] via $I_{x,\text{coll.}} = a\omega + c\omega^3$. The determined parameter is incorporated into the net aligned angular momentum for a given spin $J^{i,f}$ of the state: $i_x = I_x - I_{x,\text{coll.}}$, where $I_x = (I_x^i + I_x^f)/2$ with $I^{i,f} = \sqrt{J^{i,f}(J^{i,f}+1)}$. Starting from the midshell ^{122}Ba, proton and neutron-hole align in a continuous way along the yrast line. Blocking arguments are used to assign the first alignment to a proton crossing [25]. In ^{124}Ba the yrast sequence above the $J^\pi = 10^+$ state splits into two streched $E2$ cascades with two distinct alignments. According to blocking arguments and by comparing crossing frequencies in neighboring nuclei ^{125}Ba and ^{125}Cs, the alignment in ^{124}Ba with the lower critical frequency was assigned to a pair of $h_{11/2}$ protons, while the alignment with the higher critical frequency is generated by a $h_{11/2}$ neutron-hole pair [26].

The band structure in ^{126}Ba has similar character like the one in ^{124}Ba. Calculated routhians indicate a higher crossing frequency for neutron-hole pairs than for proton pairs in ^{126}Ba [27]. Since the two S bands in ^{128}Ba are degenerated, no unambiguous assignment is possible [28,29]. A change in the nuclear structure is observed in ^{130}Ba where four $J = 10^+$ states are observed within a small energy range of 343 keV. Two $J = 10^+$ states are the bandheads of the S bands. Cranking calculations suggest that the proton alignment occurs after neutron-hole alignment [30]. A negative g factor of the $J^\pi = 10^+$ state unambiguously assigned a neutron-hole $\nu h_{11/2}^{-2}$ configuration to the S band in ^{132}Ba [31]. This assignment was confirmed by calculations within the framework of pair-truncated shell-model approach [32]. So far, no evidence for proton alignment was reported in literature for ^{132}Ba.

While the net aligned angular momentum plot for the S band originating from neutron-hole alignment is shown in Fig. 9(a), the similar plot for proton alignment is displayed in Fig. 9(b). Overall, the alignment pattern of ^{132}Ba shows a considerable similarity with respect to ^{134}Ba [cf. Fig. 9(a)]. The crossing frequency at which the alignment occurs is mass dependent in both cases. Figure 9(c) shows a summary of

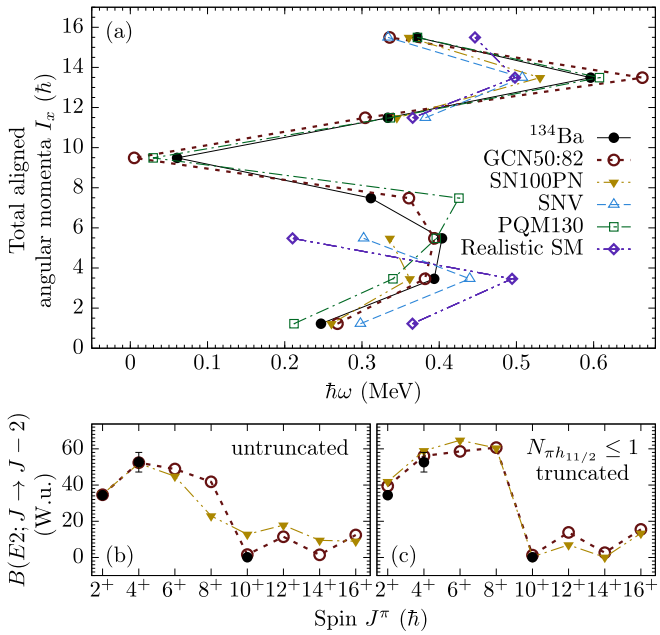

FIG. 10. (a) Comparison between experimental and calculated total aligned angular momenta I_x as a function of the rotational frequency $\hbar\omega$, employing GCN50:82, SN100PN, SNV, PQM130, and Realstic SM calculations for ^{134}Ba. Only a partial comparison with SN100PN and SNV is displayed since both interactions predict the $J^\pi = 8^+_1$ state above the $J^\pi = 10^+_1$ state. [(b) and (c)] Calculated reduced quadrupole transition strengths for yrast $B(E2)$ values employing the GCN50:82 and SN100PN interactions. Experimental values are visualized as black filled dots, taken from Refs. [45,48]. (b) The first calculations use the complete *gdsh* valence space; (c) the second prohibit more than one proton in the $\pi h_{11/2}$ orbital.

experimentally determined crossing frequencies between S bands and the ground-state bands for proton and neutron-hole alignment as a function of neutron number along Ba isotopes. Since the proton alignment increases and the neutron alignment decreases with mass number, the new determined crossing frequency in ^{134}Ba matches the systematics of neutron-hole alignment. Consequently, in accordance with the similarity with the neutron-hole alignment in ^{132}Ba [cf. Fig. 9(a)], it is reasonable to assign the band crossing in ^{134}Ba to neutron-hole $\nu h^{-2}_{11/2}$ alignment.

To further inspect the above-mentioned alignment properties in ^{134}Ba, the results of the shell-model calculations are reparametrized into the total aligned angular momenta I_x as a function of the rotational frequency $\hbar\omega$. Figure 10(a) compares the extracted theoretical and experimental total aligned angular momenta for all five calculations. Calculated I_x values for the $J^\pi = 8^+_1$ and 10^+_1 states of the SNV, SN100PN, and Realistic SM interactions are not considered, since all three interactions have a reversed ordering of both states. The critical frequency at which alignment occurs is slightly underestimated by the SN100PN interaction, while the SNV and Realistic SM interactions overpredict the alignment frequency slightly. Overall, GCN50:82 yields the best agreement with the experimental critical frequency. Both GCN50:82 and PQM130 interactions tend to slightly underpredict the minimal rotational frequency at the position of the $J^\pi = 10^+$ state. The experimentally observed second alignment at the $J^\pi = 16^+$ state is predicted correctly by all calculations. In fact, all five theoretical calculations provide a fair agreement of the experimental backbending pattern in ^{134}Ba.

It is well known, that reduced transition strength values $B(E2; J^\pi \rightarrow J^\pi - 2)$ are reduced in the vicinity of the backbending region [98]. Consequently, calculated $B(E2)$ values serve as test for the predictive power of shell-model calculations for nucleon alignment. In Fig. 10(b), calculated $B(E2)$ values along the positive-parity yrast band are compared to available experimental data in ^{134}Ba [45,48]. The SN100PN and the GCN50:82 interactions are employed using effective charges of $e_\pi = 1.75e$ and $e_\nu = 0.75e$. They are optimized to reproduce the $B(E2; 2^+ \rightarrow 0^+)$ and $B(E2; 4^+ \rightarrow 2^+)$ values. Both interactions are capable to predict the continuous drop of transition strength from the $J^\pi = 4^+$ state to the isomeric $J^\pi = 10^+$ state. Going to higher spins, low $B(E2)$ values prevail beyond the $J^\pi = 10^+$ state for both interactions.

The role of the $\pi h_{11/2}$ and $\nu h_{11/2}$ orbitals are scrutinized by a separate calculation by prohibiting more than one proton in the $\pi h_{11/2}$ orbital. Using this truncation, proton alignment components are prevented in the calculations. Results of calculated $B(E2)$ values are presented in Fig. 10(c). Obviously, the overall result is very similar to the untruncated calculation; the good agreement with respect to the experimental values remain unaltered. Moreover, the truncated results of both interactions resembles each other. The decreasing trend of the $B(E2)$ values at spin $6\hbar$ and $8\hbar$ is interrupted by this truncation. The increase of the $B(E2)$ values at spin $6\hbar$ and $8\hbar$ indicate that proton components are crucial to describe both states. On the other hand, $B(E2)$ values between states above the $J^\pi = 10^+$ isomer are unaffected by the truncation, underpinning the assumption that these states are predominantly of neutron character with negligible proton $h_{11/2}$ configuration admixture. This observation is in accordance with the negative measured g factor of the $J^\pi = 10^+$ state by Bell *et al.* [45]. It is concluded that proton components play a critical role at the beginning of the alignment process at the $J^\pi = 6^+$ state and subsequently two-neutron $h_{11/2}$ alignment becomes pivotal above the $J^\pi = 10^+$ state.

B. ^{133}Ba

The level structure of the even-odd isotope ^{133}Ba is more complex in comparison to the even-even partner ^{134}Ba. Since $B(E1)$ transition strength values cannot be evaluated in the $0g_{7/2}1d_{5/2}1d_{3/2}2s_{1/2}0h_{11/2}$ valence space, a microscopic discussion of the isomeric property of the $J^\pi = 19/2^+$ state is presented in the following by the GCN50:82, SN100PN, and SNV calculations. Subsequently, results from a truncated calculation including the neutron $\nu 1f_{7/2}$ orbital are discussed using EPQQM. An untruncated calculation in the $gdsh + \nu(1f_{7/2}2p_{3/2})$ valence space is not feasible since the m-scheme dimension would exceed the nowadays computational limits of approximately 10^{11}.

The calculated excitation energy of each positive-negative parity state as a function of the angular momentum J were

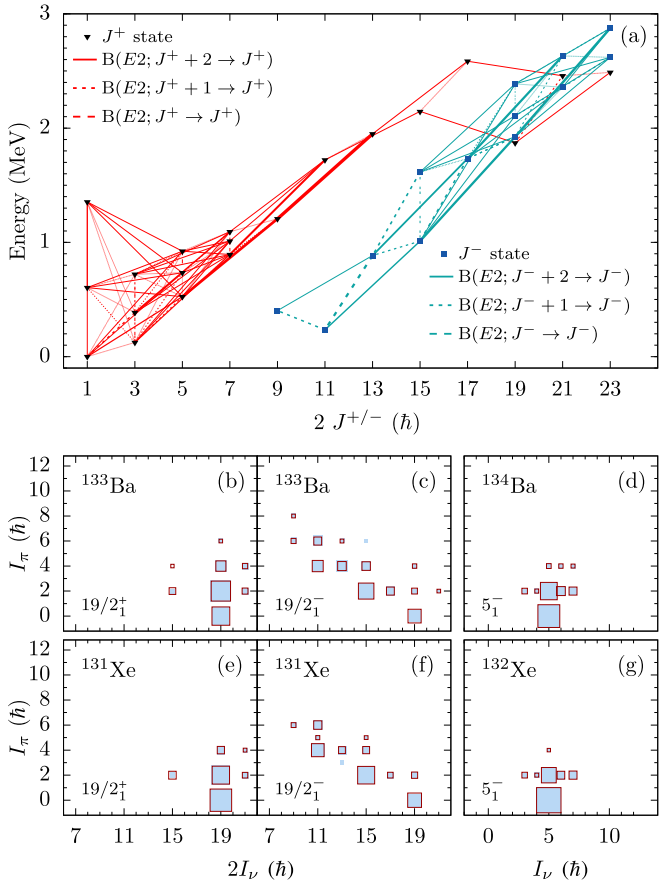

FIG. 11. (a) $E2$ map: Calculated excitation energy against spin of positive- and negative-parity states of ^{133}Ba obtained by the SNV calculation. The widths indicate the $E2$ transition probabilities. Decomposition of the total angular momentum $I_\pi \otimes I_\nu$ in their proton and neutron components for $J^\pi = 19/2^+_1$ and $J^\pi = 19/2^-_1$ states in [(b) and (c)] ^{133}Ba and [(e) and (f)] ^{131}Xe, employing the GCN50:82 (filled blue boxes) and the SN100PN interaction (empty red boxes). $J^\pi = 19/2^+_1$ states arise from couplings of a $h^{-1}_{11/2}$ neutron-hole to the $J^\pi = 5^-$ states in (d) ^{134}Ba and (g) ^{132}Xe.

computed utilizing the SNV interaction. A so-called $E2$ map [76] of the results is shown in Fig. 11(a). States are connected with lines. The linewidths are proportional to the $B(E2)$ strength between the states. The adopted effective charges are $1.6e$ and $0.8e$ for protons and neutrons, respectively. The SNV interaction predicts the $J^\pi = 19/2^+$ state at 1870 keV, which is in good agreement with the experimental value of 1942 keV. Other positive-parity states with spins $15/2\hbar$ and $17/2\hbar$ are predicted at excitation energies of 2145 and 2585 keV, which is significantly higher than the excitation energy of the $J^\pi = 19/2^+$ state. Consequently, the $J^\pi = 19/2^+$ state cannot decay into another positive-parity state and becomes a spin-gap isomer.

A similar isomeric $J^\pi = 19/2^+$ state with a half-life of 14(3) ns was observed in the $-2p$ isotone ^{131}Xe [14]. Figures 11(b) and 11(c) and Figs. 11(e) and 11(f) show the decomposition of the total angular momentum $I_\pi \otimes I_\nu$ in proton and neutron components for $J^\pi = 19/2^+_1$ and $19/2^-_1$ states in ^{133}Ba and ^{131}Xe, employing the GCN50:82 (filled blue boxes) and the SN100PN interactions (empty red boxes). No significant deviations between both calculations are visible. Differences have been observed very recently in ^{136}Ba [96]. The experimental energy gaps between both states are 189 keV in ^{131}Xe and 83 keV in ^{133}Ba. Theoretical values are higher with 362 and 188 keV in ^{131}Xe (GCN50:82 and SN100PN) and 249 and 164 keV in ^{133}Ba. Both interactions predict the $J^\pi = 19/2^+$ state to have predominant $\nu_{19/2^+} \otimes \pi_{0^+}$ spin configuration. Neutron $\nu(h^{-2}_{11/2}s^{-1}_{1/2}d^{-2}_{3/2})$ components account for 29 and 31% (GCN50:82 and SN100PN) in ^{131}Xe and 22 and 24% in ^{133}Ba. Significant proton couplings to this neutron configuration are 7/16% $\pi(g^4_{7/2})$ and 9/8% $\pi(g^2_{7/2}d^2_{5/2})$ in ^{131}Xe and 9/12% $\pi(g^4_{7/2}d^2_{5/2})$ in ^{133}Ba.

TABLE III. Average occupation numbers for protons (π) and neutrons (ν) in each single-particle orbit of the *gdsh* model space for $J^\pi = 19/2^+$ and $19/2^-$ states in ^{133}Ba employing the EPQQM interaction.

J^π	π/ν	$0g_{7/2}$	$1d_{5/2}$	$1d_{3/2}$	$2s_{1/2}$	$0h_{11/2}$	$1f_{7/2}$
		Untruncated calculation without cross-shell					
$19/2^+_1$	π	3.59	2.17	0.16	0.06	0.03	–
$19/2^+_1$	ν	7.73	5.57	2.37	1.35	9.97	–
$19/2^-_1$	π	3.83	1.67	0.28	0.17	0.05	–
$19/2^-_1$	ν	7.81	5.74	2.88	1.55	9.02	–
		Truncated calculation with cross-shell					
$19/2^+_1$	π	3.91	2.09	–	–	–	–
$19/2^+_1$	ν	7.67	5.48	2.51	1.35	9.77	0.22
$19/2^-_1$	π	3.95	2.05	–	–	–	–
$19/2^-_1$	ν	7.81	5.73	2.94	1.52	8.81	0.20

The $J^\pi = 19/2^-$ states in ^{131}Xe and ^{133}Ba have a fragmented pattern of proton and neutron components as visible in Figs. 11(c) and 11(f). The spin mainly arises from couplings of $\nu_{19/2^-} \otimes \pi_{0^+}$, $\nu_{15/2^-} \otimes \pi_{2^+}$, and $\nu_{11/2^-} \otimes \pi_{4^+}$. The dominant configuration is attributed to 9/7% $\nu(h^{-3}_{11/2}d^{-2}_{3/2}) \otimes \pi(g^2_{7/2}d^2_{5/2})$ in ^{131}Xe and 7/9% $\nu(h^{-3}_{11/2}d^{-2}_{3/2}) \otimes \pi(g^4_{7/2}d^2_{5/2})$ in ^{133}Ba. The isomeric character can be traced back to the stretched neutron spin $\nu_{19/2^+}$ of the $J^\pi = 19/2^+$ state, which hinders a decay into the $\nu_{11/2^-}$ components of the $J^\pi = 19/2^-$ state in both nuclei. Overall, the $J^\pi = 19/2^+$ and $19/2^-$ states have very similar structures in both nuclei. Consequently, the additional proton pair of ^{133}Ba is mainly paired with respect to ^{131}Xe.

Two refined calculations using the EPQQM interaction are employed: (i) an untruncated calculation without cross-shell excitations comprising the *gdsh* valence space and (ii) a truncated calculation prohibiting proton excitations into the $1d_{3/2}$, $2s_{1/2}$, and $0h_{11/2}$ orbitals but allowing cross-shell excitations into the neutron $1f_{7/2}$ orbital. The upper part of Table III shows the untruncated calculated occupation numbers of protons and neutrons for the $J^\pi = 19/2^+$ and $19/2^-$ states in ^{133}Ba. The EPQQM results confirm the leading configurations of $\nu(h^{-2}_{11/2}s^{-1}_{1/2})$ ($N_{\nu h_{11/2}} = 9.97$, $N_{\nu s_{1/2}} = 1.35$) for initial $J^\pi = 19/2^+$ state and of $\nu(h^{-3}_{11/2})$ ($N_{\nu h_{11/2}} = 9.02$) for final $J^\pi = 19/2^-$ state consistently with the other calculations

TABLE IV. Average neutron occupation numbers in each single-particle orbit of the *gdsh* model space in ^{133}Ba and ^{134}Ba, calculated using the GCN50:82 and SNV interactions.

Isotope	J^π	$0g_{7/2}$	$1d_{5/2}$	$1d_{3/2}$	$2s_{1/2}$	$0h_{11/2}$
		GCN50:82				
^{133}Ba	$19/2^+_1$	7.76	5.73	2.28	1.39	9.84
^{134}Ba	5^-_1	7.78	5.73	2.46	1.35	10.69
		SNV				
^{133}Ba	$19/2^+_1$	7.87	5.53	2.23	1.35	9.92
^{134}Ba	5^-_1	7.88	5.56	2.33	1.37	10.87

(cf. Table IV in discussion below). The $J^\pi = 19/2^+$ state is calculated to have 1.94 MeV excitation energy which is in excellent agreement with the experimental value.

In addition, the valence space is enlarged by the neutron $1f_{7/2}$ orbital. In order to make the dimension of the configuration space tractable, proton excitations into the $1d_{3/2}$, $2s_{1/2}$, and $0h_{11/2}$ orbitals are forbidden, which is reasonable since the corresponding occupation is neglected small and EPQQM predicts a high degree of $g_{7/2}$ and $d_{5/2}$ occupation for protons at both states (see Table III). Applying this truncation, the excitation energy of the $J^\pi = 19/2^+_1$ state is slightly shifted to 1.75 MeV. The impact of the truncation and the inclusion of the $1f_{7/2}$ orbital on the calculated average occupation numbers is visualized in the lower part of Table III.

The occupation of the $1f_{7/2}$ orbital amounts to approximately 0.2. The pure two ($N_{\nu h_{11/2}} = 9.97$) and three ($N_{\nu h_{11/2}} = 9.02$) neutron-hole configuration from the untruncated calculation of initial and final states is rearranged in favor of the $\nu 1f_{7/2}$ occupation (cf. $N_{\nu h_{11/2}} = 9.77$ for inital and $N_{\nu h_{11/2}} = 8.81$ for final states). The $E1$ transition operator between both states is driven by the share of $1f_{7/2}$ cross-shell configurations. Thus, it has a perturbative but decisive role for a detailed description of the overall configuration of these states. The theoretical $B(E1; 19/2^+_1 \rightarrow 19/2^-_1)$ transition strength is computed to be $5 \times 10^{-4}\ e^2\,\mathrm{fm}^2$. Effective charges of $e_\pi = 1.7$ and $e_\nu = 0.7$ were employed. The theoretical $B(E1)$ value overpredicts the experimental value of $7.7(4) \times 10^{-6}\ e^2\,\mathrm{fm}^2$ by almost two orders of magnitude.

In Refs. [10,19,23] it was suggested that the $J^\pi = 19/2^+$ states in odd-mass nuclei along $N = 77$ arise from couplings of a neutron-hole to the $J^\pi = 5^-$ state in even-mass $N = 78$ nuclei. As mentioned above in Sec. IV A, the leading configuration of the $J^\pi = 5^-$ state in ^{134}Ba is $\nu(s^{-1}_{1/2}h^{-1}_{11/2})$ generating fully stretched $\nu_{5^-} \otimes \pi_{0^+}$ and $\nu_{5^-} \otimes \pi_{2^+}$ spin contributions. [see Fig. 11(d)]. The same applies for ^{132}Xe as shown in Fig. 11(g). In accordance with the Pauli principle, an additional $h_{11/2}$ neutron-hole couples with a spin of $9/2\hbar$ to this configuration. Consequently, the spin decompositions of both states are very similar but those of the $J^\pi = 19/2^+$ state is shifted by a neutron spin of $9/2\hbar$ with respect to the $J^\pi = 5^-$ state in both nuclei. The leading $\nu(h^{-2}_{11/2}s^{-1}_{1/2})$ configuration of the $J^\pi = 19/2^+$ state in ^{133}Ba and the connection to the $J^\pi = 5^-$ isomer in ^{134}Ba are scrutinized by investigating the evolution of calculated average occupation numbers of neutrons in the *gdsh* model space for $J^\pi = 19/2^+$ and 5^- isomers in ^{133}Ba and ^{134}Ba, respectively, as listed in Table IV. The average occupation of the neutron $h_{11/2}$ orbital for the $J^\pi = 5^-$ state in ^{134}Ba is $N_\nu \approx 10.78$ indicating a one-neutron $\nu h^{-1}_{11/2}$ configuration. A partial occupation of the $\nu s_{1/2}$ orbital ($N_\nu \approx 1.36$) supports a predominant $\nu h^{-1}_{11/2}s^{-1}_{1/2}$ configuration. Compared to this, a decrease to $N_\nu \approx 9.88$ for the $\nu h_{11/2}$ orbital of the $J^\pi = 19/2^+$ state is observed, while the occupation of the remaining orbitals stays constant. These observations and the aforementioned disscusion of spin contributions corroborates that the $J^\pi = 19/2^+$ state arises predominatly from a coupling of a neutron-hole and the $J^\pi = 5^-$ state in ^{134}Ba, as suggested in Refs. [10,19,23].

V. CONCLUSIONS

In summary, two experiments employing the ^{136}Xe + ^{208}Pb multinucleon-transfer reaction and the ^{13}C + ^{124}Sn fusion-evaporation reaction were used to measure half-lives of high-spin isomers in ^{133,134}Ba and to establish new high-spin states in ^{134}Ba. The level scheme of ^{134}Ba was extended to approximately 6 MeV. A pronounced backbending along the positive-parity yrast band was identified at around $\hbar\omega = 0.38$ MeV. Comparisons with crossing frequencies along the even-Ba chain indicated that the backbending can be traced back to neutron alignment. In general, the new experimental results such as the backbending phenomena are reproduced by the GCN50:82 and PQM130 interactions; however, SNV, SN100PN, and Realistic SM predict the $J^\pi = 8^+$ state slightly above the $J^\pi = 10^+$ isomer. A detailed inspection using truncated calculations for ^{134}Ba reveals that the alignment of yrast states above the $J^\pi = 10^+$ isomer is clearly of neutron character. Beside previous investigations in few other nuclei, like ^{132}Ba [41], ^{132,134,136}Ce [42], and ^{131}Xe [13], these results demonstrate convincingly the applicability of modern shell-model interactions in order to describe the interplay between single-particle and collective excitation in this transitional region which arises from the specific $h_{11/2}$ intruder orbital. Backbending and alignment properties are traced back to the wave function and their decomposition into specific single particle contributions.

The previously evaluated half-life of 2–5 ns for the 1942-keV state in ^{133}Ba was revised to $T_{1/2} = 66.6(20)$ ns. The new half-life of this isomeric state completes the systematics of $J^\pi = 19/2^+$ isomers for the $N = 77$ isotones. Large-scale shell-model calculations using the SNV, GCN50:82, and SN100PN have been performed to explain the level structure of ^{133}Ba and the underlying configuration of the measured $J^\pi = 19/2^+$ isomer. The calculations point out that the isomer can be interpreted as predominant $^{134}\mathrm{Ba}(5^-_1) \otimes \nu(0h^{-1}_{11/2})$ configuration. A truncated calculation using EPQQM in an enlarged valence space yield a $B(E1; 19/2^+_1 \rightarrow 19/2^-_1)$ value which is two orders of magnitude too high compared to the experimental value. In the future, untruncated calculations in the full *gdsh* valence space incorporating cross-shell configuration $\nu 1f_{1/2}$ and $\nu 2p_{3/2}$ are of highest interest to provide a more complete description of the $50 \leqslant Z, N \leqslant 82$ nuclei.

ACKNOWLEDGMENTS

We thank the IKP FN tandem accelerator team for the support during the experiment. The research leading to these results has received funding from the German BMBF under Contracts No. 05P15PKFN9 TP1 and No. 05P18PKFN9 TP1, from the European Union Seventh Framework Programme FP7/2007-2013 under Grant No. 262010-ENSAR, from the Spanish Ministerio de Ciencia e Innovación under Contract No. FPA2011-29854-C04, from the Spanish Ministerio de Economía y Competitividad under Contract No. FPA2014-57196-C5, and from the U.K. Science and Technology Facilities Council (STFC). One of the authors (A. Gadea) has been supported by the Generalitat Valenciana, Spain, under Grant No. PROMETEOII/2014/019 and EU under the FEDER program.

[1] E. Caurier, F. Nowacki, A. Poves, and K. Sieja, Collectivity in the light xenon isotopes: A shell model study, Phys. Rev. C **82**, 064304 (2010).

[2] E. Caurier, F. Nowacki, and A. Poves, Shell Model description of the $\beta\beta$ decay of ^{136}Xe, Phys. Lett. B **711**, 62 (2012).

[3] B. A. Brown, N. J. Stone, J. R. Stone, I. S. Towner, and M. Hjorth-Jensen, Magnetic moments of the 2_1^+ states around ^{132}Sn, Phys. Rev. C **71**, 044317 (2005).

[4] Md. S. R. Laskar, S. Saha, R. Palit, S. N. Mishra, N. Shimizu, Y. Utsuno, E. Ideguchi, Z. Naik, F. S. Babra, S. Biswas, S. Kumar, S. K. Mohanta, C. S. Palshetkar, P. Singh, and P. C. Srivastava, g-factor measurement of the 2738 kev isomer in ^{135}La, Phys. Rev. C **99**, 014308 (2019).

[5] E. Teruya, N. Yoshinaga, K. Higashiyama, and A. Odahara, Shell-model calculations of nuclei around mass 130, Phys. Rev. C **92**, 034320 (2015).

[6] K. Higashiyama and N. Yoshinaga, Pair-truncated shell-model analysis of nuclei around mass 130, Phys. Rev. C **83**, 034321 (2011).

[7] L. Coraggio, A. Covello, A. Gargano, N. Itaco, and T. T. S. Kuo, Effective shell-model hamiltonians from realistic nucleon-nucleon potentials within a perturbative approach, Ann. Phys. **327**, 2125 (2012).

[8] L. Coraggio, A. Covello, A. Gargano, N. Itaco, and T. T. S. Kuo, Shell-model calculations and realistic effective interactions, Prog. Part. Nucl. Phys. **62**, 135 (2009).

[9] H.-K. Wang, S. K. Ghorui, K. Kaneko, Y. Sun, and Z. H. Li, Large-scale shell-model study for excitations across the neutron $N = 82$ shell gap in $^{131-133}$Sb, Phys. Rev. C **96**, 054313 (2017).

[10] J. A. Pinston, C. Foin, J. Genevey, R. Béraud, E. Chabanat, H. Faust, S. Oberstedt, and B. Weiss, Microsecond isomers in ^{125,127,129}Sn, Phys. Rev. C **61**, 024312 (2000).

[11] R. L. Lozeva, G. S. Simpson, H. Grawe, G. Neyens, L. A. Atanasova, D. L. Balabanski, D. Bazzacco, F. Becker, P. Bednarczyk, G. Benzoni, N. Blasi, A. Blazhev, A. Bracco, C. Brandau, L. Cáceres, F. Camera, S. K. Chamoli, F. C. L. Crespi, J.-M. Daugas, P. Detistov, M. De Rydt, P. Doornenbal, C. Fahlander, E. Farnea, G. Georgiev, J. Gerl, K. A. Gladnishki, M. Górska, J. Grębosz, M. Hass, R. Hoischen, G. Ilie, M. Ionescu-Bujor, A. Iordachescu, J. Jolie, A. Jungclaus, M. Kmiecik, I. Kojouharov, N. Kurz, S. P. Lakshmi, G. Lo Bianco, S. Mallion, A. Maj, D. Montanari, O. Perru, M. Pfützner, S. Pietri, J. A. Pinston, Zs. Podolyák, W. Prokopowicz, D. Rudolph, G. Rusev, T. R. Saitoh, A. Saltarelli, H. Schaffner, R. Schwengner, S. Tashenov, K. Turzó, J. J. Valiente-Dobón, N. Vermeulen, J. Walker, E. Werner-Malento, O. Wieland, and H.-J. Wollersheim, New sub-μs isomers in ^{125,127,129}Sn and isomer systematics of $^{124-130}$Sn, Phys. Rev. C **77**, 064313 (2008).

[12] C. T. Zhang, P. Bhattacharyya, P. J. Daly, Z. W. Grabowski, R. H. Mayer, M. Sferrazza, R. Broda, B. Fornal, W. Krolas, T. Pawlat, D. Bazzacco, S. Lunardi, C. Rossi Alvarez, and G. de Angelis, Yrast excitations in $A = 126 - 131$Te nuclei from deep inelastic ^{130}Te + ^{64}Ni reactions, Nucl. Phys. A **628**, 386 (1998).

[13] L. Kaya, A. Vogt, P. Reiter, M. Siciliano, B. Birkenbach, A. Blazhev, L. Coraggio, E. Teruya, N. Yoshinaga, K. Higashiyama, K. Arnswald, D. Bazzacco, A. Bracco, B. Bruyneel, L. Corradi, F. C. L. Crespi, G. de Angelis, J. Eberth, E. Farnea, E. Fioretto, C. Fransen, B. Fu, A. Gadea, A. Gargano, A. Giaz, A. Görgen, A. Gottardo, K. Hadyńska-Klęk, H. Hess, R. Hetzenegger, R. Hirsch, N. Itaco, P. R. John, J. Jolie, A. Jungclaus, W. Korten, S. Leoni, L. Lewandowski, S. Lunardi, R. Menegazzo, D. Mengoni, C. Michelagnoli, T. Mijatović, G. Montagnoli, D. Montanari, C. Müller-Gatermann, D. Napoli, Zs. Podolyák, G. Pollarolo, A. Pullia, M. Queiser, F. Recchia, D. Rosiak, N. Saed-Samii, E. Şahin, F. Scarlassara, D. Schneiders, M. Seidlitz, B. Siebeck, J. F. Smith, P.-A. Söderström, A. M. Stefanini, T. Steinbach, O. Stezowski, S. Szilner, B. Szpak, C. Ur, J. J. Valiente-Dobón, K. Wolf, and K. O. Zell, High-spin structure in the transitional nucleus ^{131}Xe: Competitive neutron and proton alignment in the vicinity of the $N = 82$ shell closure, Phys. Rev. C **98**, 014309 (2018).

[14] A. Kerek, A. Luukko, M. Grecescu, and J. Sztarkier, Two- and three-quasiparticle states in ^{132}Xe and ^{131}Xe, Nucl. Phys. A **172**, 603 (1971).

[15] E. A. Henry and R. A. Meyer, Decay of 3.912-h ^{133}La to ^{133}Ba and level structure of the $N = 77$ nuclei, Phys. Rev. C **13**, 2501 (1976).

[16] D. von Ehrenstein, G. C. Morrison, J. A. Nolen, and N. Williams, Study of the (d, p) reaction on the even-A barium isotopes 130-138, Phys. Rev. C **1**, 2066 (1970).

[17] A. Y. Dauenhauer and K. S. Krane, Neutron capture cross sections of ^{130,132,134,136,138}Ba, Phys. Rev. C **85**, 064301 (2012).

[18] J. M. Cork and Gail P. Smith, Radioactive isotopes of barium from cesium, Phys. Rev. **60**, 480 (1941).

[19] J. Gizon, A. Gizon, and D.J. Horen, Band structure in ^{131,132,133}Ba observed by (^{12}C, xn) reactions, Nucl. Phys. A **252**, 509 (1975).

[20] S. Juutinen, P. Šimeček, P. Ahonen, M. Carpenter, C. Fahlander, J. Gascon, R. Julin, A. Lampinen, T. Lönnroth, J. Nyberg, A. Pakkanen, M. Piiparinen, K. Schiffer, G. Sletten, S. Törmänen, and A. Virtanen, Shape coexistence in the transitional ^{133}Ba nucleus, Phys. Rev. C **51**, 1699 (1995).

[21] T. Morek, H. Beuscher, B. Bochev, D. R. Haenni, R. M. Lieder, T. Kutsarova, M. Muller-Veggian, and A. Neskakis, Isomeric states in ^{134}Ba, Z. Phys. A **298**, 267 (1980).

[22] A. Zemel, C. Broude, E. Dafni, A. Gelberg, M. B. Goldberg, J. Gerber, G. J. Kumbartzki, and K. H. Speidel, Magnetic moment of the $19/2^+$ isomer in ^{135}Ce, Z. Phys. A **304**, 269 (1982).

[23] J. Gizon, A. Gizon, M. R. Maier, R. M. Diamond, and F. S. Stephens, Deformed states of neutron-deficient cerium and neodymium nuclei, Nucl. Phys. A **222**, 557 (1974).

[24] R. O. Sayer, J. S. Smith, and W. T. Milner, Rotational and quasirotational bands in even-even nuclei, At. Data Nucl. Data Tables **15**, 85 (1975).

[25] R. Wyss, A. Granderath, R. Bengtsson, P. von Brentano, A. Dewald, A. Gelberg, A. Gizon, J. Gizon, S. Harissopulos, A. Johnson, W. Lieberz, W. Nazarewicz, J. Nyberg, and K. Schiffer, Interplay between proton and neutron S-bands in the Xe-Ba-Ce-region, Nucl. Phys. A **505**, 337 (1989).

[26] J. P. Martin, V. Barci, H. El-Samman, A. Gizon, J. Gizon, W. Klamra, B. M. Nyak'o, F. A. Beck, Th. Byrski, and J. C. Merdinger, Collective band structures and particle alignments in ^{124}Ba, ^{125}Ba and ^{125}Ce, Nucl. Phys. A **489**, 169 (1988).

[27] D. Ward, V. P. Janzen, H. R. Andrews, D. C. Radford, G. C. Ball, D. Horn, J. C. Waddington, J. K. Johansson, F. Banville, J. Gascon, S. Monaro, N. Nadon, S. Pilotte, D. Prevost, P. Taras, and R. Wyss, Gamma-ray spectroscopy of ^{126}Ba, Nucl. Phys. A **529**, 315 (1991).

[28] K. Schiffer, A. Dewald, A. Gelberg, R. Reinhardt, K. O. Zell, S. Xiangfu, and P. von Brentano, Band crossings in ^{128}Ba, Nucl. Phys. A **458**, 337 (1986).

[29] H. Wolters, K. Schiffer, A. Gelberg, A. Dewald, J. Eberth, R. Reinhardt, K. O. Zell, P. V. Brentano, D. Alber, and H. Grawe, High spin states in ^{128}Ba, Z. Phys. A **328**, 15 (1987).

[30] S. Xiangfu, D. Bazzacco, W. Gast, A. Gelberg, U. Kaup, A. Dewald, K. O. Zell, and P. von Brentano, Band crossing in ^{130}Ba, Phys. Rev. C **28**, 1167 (1983).

[31] S. Harissopulos, A. Gelberg, A. Dewald, M. Hass, L. Weissman, and C. Broude, Measurement of the magnetic moment of the 10^+ isomer in ^{132}Ba, Phys. Rev. C **52**, 1796 (1995).

[32] K. Higashiyama, N. Yoshinaga, and K. Tanabe, Pair-truncated shell-model approach to backbending and low-lying states in ^{132}Ba, Phys. Rev. C **67**, 044305 (2003).

[33] N. Yoshida, A. Arima, and T. Otsuka, Description of high-spin states in the interacting boson model, Phys. Lett. B **114**, 86 (1982).

[34] R. F. Casten and P. von Brentano, An extensive region of $O(6)$-like nuclei near $A = 130$, Phys. Lett. B **152**, 22 (1985).

[35] K. Nomura, T. Nikšić, and D. Vretenar, Shape-phase transitions in odd-mass γ-soft nuclei with mass $A \approx 130$, Phys. Rev. C **96**, 014304 (2017).

[36] A. Granderath, P. F. Mantica, R. Bengtsson, R. Wyss, P. von Brentano, A. Gelberg, and F. Seiffert, Shapes and rotational structures of neutron $h_{11/2}$ configurations in the Xe-Ba-Ce region, Nucl. Phys. A **597**, 427 (1996).

[37] L. M. Robledo, R. R. Rodríguez-Guzmán, and P. Sarriguren, Evolution of nuclear shapes in medium mass isotopes from a microscopic perspective, Phys. Rev. C **78**, 034314 (2008).

[38] C.-B. Moon, C. S. Lee, T. Komatsubara, Y. Sasaki, and K. Furuno, Structure of the negative parity bands in ^{125}Xe, Phys. Rev. C **76**, 067301 (2007).

[39] Y. Huang, Z. G. Xiao, S. J. Zhu, C. Qi, Q. Xu, W. J. Cheng, H. J. Li, L. M. Lyu, R. S. Wang, W. H. Yan, H. Yi, Y. Zhang, Q. M. Chen, C. Y. He, S. P. Hu, C. B. Li, H. W. Li, P. W. Luo, X. G. Wu, Y. H. Wu, Y. Zheng, and J. Zhong, High-spin structures in the ^{129}Xe nucleus, Phys. Rev. C **93**, 064315 (2016).

[40] K. Higashiyama, N. Yoshinaga, and K. Tanabe, Shell model study of backbending phenomena in Xe isotopes, Phys. Rev. C **65**, 054317 (2002).

[41] Y. Lei and Z. Y. Xu, $(h_{11/2})^2$ alignments in neutron-rich ^{132}Ba with negative-parity pairs, Phys. Rev. C **92**, 014317 (2015).

[42] T. Takahashi, N. Yoshinaga, and K. Higashiyama, Backbending phenomena in ^{132,134,136}Ce with a pair-truncated shell model, Phys. Rev. C **71**, 014305 (2005).

[43] H. F. Brinckmann, C. Heiser, and W. D. Fromm, Ein Hochangeregter isomerer Kernzustand in ^{132}Xe, Nucl. Phys. A **96**, 318 (1967).

[44] Yu. Khazov, A. A. Rodionov, S. Sakharov, and B. Singh, Nuclear Data Sheets for $A = 132$, Nucl. Data Sheets **104**, 497 (2005).

[45] C. Bell, P. Raghavan, Y. Niv, D. E. Murnick, and P. Pappas, Lifetime and g-factor of the 10^+ isomeric state ^{134}Ba, Bull. Am. Phys. Soc. **27**, DF10 (1982).

[46] N. J. Stone, Table of nuclear magnetic dipole and electric quadrupole moments, At. Data Nucl. Data Tables **90**, 75 (2005).

[47] J. Burde, S. Eshhar, A. Ginzburg, and A. Molchadzki, Absolute transition probabilities in ^{134}Ba, Nucl. Phys. A **250**, 141 (1975).

[48] A. M. Kleinfeld, A. Bockisch, and K.P. Lieb, Reorientation effect and multiple coulomb excitation measurements of ^{134}Ba, Nucl. Phys. A **283**, 526 (1977).

[49] B. Fazekas, T. Belgya, G. Molnar, A. Veres, R. A. Gatenby, S. W. Yates, and T. Otsuka, Level scheme and mixed-symmetry states of ^{134}Ba from in-beam $(n, n'\gamma)$ measurements, Nuc. Phys. A **548**, 249 (1992).

[50] Evaluated Nuclear Structure Data File (ENSDF), http://www.nndc.bnl.gov/ensdf.

[51] T. Lönnroth, S. Tormanen, C. Fahlander, P. Granholm, R. Julin, S. Juutinen, P. Manngard, J. Nyberg, A. Pakkanen, K. Schiffer, G. Sletten, and A. Virtanen, Coexistence of shapes in transitional ^{132,133,134}Ba, JYFL Ann. Rept. 1989-1990 (1990), p. 99.

[52] W. T. Cluff, The High-Spin Structure of ^{134,135}Ba and ^{120}Te, Ph.D. thesis, Florida State University (2008).

[53] X. Che, S. Zhu, M. Li, Y. Yu, Y. Chen, H. Ding, L. Zhu, X. Wu, G. Li, Y. Liu *et al.*, Level structure with high excitation states in ^{134}Ba, High Energy Phys. Nucl. Phys. **31**, 621 (2007).

[54] S. Akkoyun *et al.*, AGATA—Advanced GAmma Tracking Array, Nucl. Instrum. Methods A **668**, 26 (2012).

[55] A. M. Stefanini, L. Corradi, G. Maron, A. Pisent, M. Trotta, A. M. Vinodkumar, S. Beghini, G. Montagnoli, F. Scarlassara, G. F. Segato, A. De Rosa, G. Inglima, D. Pierroutsakou, M. Romoli, M. Sandoli, G. Pollarolo, and A. Latina, The heavy-ion magnetic spectrometer PRISMA, Nucl. Phys. A **701**, 217 (2002).

[56] L. Corradi, S. Szilner, G. Pollarolo, D. Montanari, E. Fioretto, A. M. Stefanini, J. J. Valiente-Dobón, E. Farnea, C. Michelagnoli, G. Montagnoli, F. Scarlassara, C. A. Ur, T. Mijatović, D. Jelavić Malenica, N. Soić, and F. Haas, Multinucleon transfer reactions: Present status and perspectives, Nucl. Instrum. Methods B **317**, 743 (2013).

[57] S. Szilner, C. A. Ur, L. Corradi, N. Marginean, G. Pollarolo, A. M. Stefanini, S. Beghini, B. R. Behera, E. Fioretto, A. Gadea, B. Guiot, A. Latina, P. Mason, G. Montagnoli, F. Scarlassara, M. Trotta, G. de Angelis, F. Della Vedova, E. Farnea, F. Haas, S. Lenzi, S. Lunardi, R. Marginean, R. Menegazzo, D. R. Napoli, M. Nespolo, I. V. Pokrovsky, F. Recchia, M. Romoli, M.-D. Salsac, N. Soić, and J. J. Valiente-Dobón, Multinucleon transfer reactions in closed-shell nuclei, Phys. Rev. C **76**, 024604 (2007).

[58] L. Netterdon, V. Derya, J. Endres, C. Fransen, A. Hennig, J. Mayer, C. Müller-Gatermann, A. Sauerwein, P. Scholz, M. Spieker, and A. Zilges, The γ-ray spectrometer HORUS and its applications for nuclear astrophysics, Nucl. Instrum. Methods A **754**, 94 (2014).

[59] J.-M. Régis, M. Dannhoff, J. Jolie, C. Müller-Gatermann, and N. Saed-Samii, On the time response of background obtained in γ-ray spectroscopy experiments using $LaBr_3$(Ce) detectors with different shielding, Nucl. Instr. Methods A **811**, 42 (2016).

[60] N. Saed-Samii, Diplomarbeit, Universität zu Köln (2013) (unpublished).

[61] R. Brun and F. Rademakers, Root-an object oriented data analysis framework, Nucl. Instrum. Methods A **389**, 81 (1997).

[62] J. Theuerkauf, Die Analyse von zwei- und mehrdimensionalen $\gamma\gamma$-Koinzidenzspektren an Beispielen aus Hochspinexperimenten in der Massengegend um ^{146}Gd, Ph.D. thesis, Universität zu Köln (1994).

[63] I. Wiedenhöver, Computer code CORLEONE (1997) (unpublished).

[64] I. Wiedenhöver, O. Vogel, H. Klein, A. Dewald, P. von Brentano, J. Gableske, R. Krücken, N. Nicolay, A. Gelberg, P. Petkov, A. Gizon, J. Gizon, D. Bazzacco, C. Rossi Alvarez, G. de Angelis, S. Lunardi, P. Pavan, D. R. Napoli, S. Frauendorf, F. Dönau, R. V. F. Janssens, and M. P. Carpenter, Detailed angular correlation analysis with 4π spectrometers: Spin determinations and multipolarity mixing measurements in ^{128}Ba, Phys. Rev. C **58**, 721 (1998).

[65] K. S. Krane and R. M. Steffen, Determination of the $E2/M1$ multipole mixing ratios of the gamma transitions in ^{110}Cd, Phys. Rev. C **2**, 724 (1970).

[66] K. S. Krane, R. M. Steffen, and R. M. Wheeler, Directional correlations of gamma radiations emitted from nuclear states oriented by nuclear reactions or cryogenic methods, At. Data Nucl. Data Tables **11**, 351 (1973).

[67] A. Linnemann, Das HORUS-Würfelspektrometer und Multiphononanregungen in ^{106}Cd, Ph.D. thesis, Universität zu Köln (2006).

[68] L. Bettermann, C. Fransen, S. Heinze, J. Jolie, A. Linnemann, D. Mücher, W. Rother, T. Ahn, A. Costin, N. Pietralla, and Y. Luo, Candidates for the one-phonon mixed-symmetry state in ^{130}Xe, Phys. Rev. C **79**, 034315 (2009).

[69] A. Gadea, E. Farnea, J. J. Valiente-Dobón, B. Million, D. Mengoni, D. Bazzacco, F. Recchia, A. Dewald, Th. Pissulla, W. Rother, G. de Angelis *et al.*, Conceptual design and infrastructure for the installation of the first AGATA sub-array at LNL, Nucl. Instrum. Methods A **654**, 88 (2011).

[70] A. Wiens, H. Hess, B. Birkenbach, B. Bruyneel, J. Eberth, D. Lersch, G. Pascovici, P. Reiter, and H.-G. Thomas, The AGATA triple cluster detector, Nucl. Instrum. Methods A **618**, 223 (2010).

[71] B. Bruyneel, B. Birkenbach, and P. Reiter, Pulse shape analysis and position determination in segmented HPGe detectors: The AGATA detector library, Eur. Phys. J. A **52**, 70 (2016).

[72] A. Lopez-Martens, K. Hauschild, A. Korichi, J. Roccaz, and J-P. Thibaud, γ-ray tracking algorithms: A comparison, Nucl. Instrum. Methods A **533**, 454 (2004).

[73] R. S. Kempley *et al.*, Cross Coincidences in the ^{136}Xe + ^{208}Pb deep-inelastic reaction, Acta. Phys. Pol. B **42**, 717 (2011).

[74] M. Siciliano *et al.*, Neutron-rich nuclei in the vicinity of ^{208}Pb, LNL Annual Report 2014 **241**, 63 (2015).

[75] S. Chakraborty, H. P. Sharma, S. S. Tiwary, C. Majumder, P. Banerjee, S. Ganguly, S. Rai, Pragati, Swati Modi, P. Arumugam, Mayank, S. Kumar, R. Palit, A. Kumar, S. S. Bhattacharjee, R. P. Singh, and S. Muralithar, Rotational band on a three-quasineutron isomer in ^{127}Xe, Phys. Rev. C **97**, 054311 (2018).

[76] B. A. Brown and W. D. M. Rae, The shell-model code NuShellX@MSU, Nucl. Data Sheets **120**, 115 (2014).

[77] N. Shimizu, Nuclear shell-model code for massive parallel computation, KSHELL (2013), arXiv:1310.5431 [nucl-ph].

[78] E. Caurier, G. Martínez-Pinedo, F. Nowacki, A. Poves, and A. P. Zuker, The shell model as a unified view of nuclear structure, Rev. Mod. Phys. **77**, 427 (2005).

[79] R. Machleidt, F. Sammarruca, and Y. Song, Nonlocal nature of the nuclear force and its impact on nuclear structure, Phys. Rev. C **53**, R1483 (1996).

[80] M. Honma, T. Otsuka, T. Mizusaki, and M. Hjorth-Jensen, Shell-model fits for Sn isotopes, RIKEN Accel. Progr. Rep. **49**, 77 (2015).

[81] M. Honma, T. Otsuka, T. Mizusaki, and M. Hjorth-Jensen, Shell-model fits for Sn isotopes, RIKEN Accel. Prog. Rep. **45**, 35 (2012).

[82] Y. Utsuno, T. Otsuka, B. A. Brown, M. Honma, T. Mizusaki, and N. Shimizu, Shape transitions in exotic Si and S isotopes and tensor-force-driven jahn-teller effect, Phys. Rev. C **86**, 051301(R) (2012).

[83] T. Otsuka, T. Suzuki, M. Honma, Y. Utsuno, N. Tsunoda, K. Tsukiyama, and M. Hjorth-Jensen, Novel Features of Nuclear Forces and Shell Evolution in Exotic Nuclei, Phys. Rev. Lett. **104**, 012501 (2010).

[84] Y. Utsuno, T. Otsuka, N. Shimizu, M. Honma, T. Mizusaki, Y. Tsunoda, and T. Abe, Recent shell-model results for exotic nuclei, EPJ Web Conf. **66**, 02106 (2014).

[85] L. Coraggio, L. De Angelis, T. Fukui, A. Gargano, and N. Itaco, Calculation of Gamow-Teller and two-neutrino double-β decay properties for ^{130}Te and ^{136}Xe with a realistic nucleon-nucleon potential, Phys. Rev. C **95**, 064324 (2017).

[86] M. Hasegawa, K. Kaneko, and S. Tazaki, Improvement of the extended p+qq interaction by modifying the monopole field, Nucl. Phys. A **688**, 765 (2001).

[87] K. Kaneko, M. Hasegawa, and T. Mizusaki, Quadrupole and octupole softness in the $N = Z$ nucleus ^{64}Ge, Phys. Rev. C **66**, 051306(R) (2002).

[88] K. Kaneko, Y. Sun, M. Hasegawa, and T. Mizusaki, Shell model study of single-particle and collective structure in neutron-rich Cr isotopes, Phys. Rev. C **78**, 064312 (2008).

[89] K. Kaneko, Y. Sun, T. Mizusaki, and M. Hasegawa, Shell-model study for neutron-rich *sd*-shell nuclei, Phys. Rev. C **83**, 014320 (2011).

[90] H.-K. Wang, Y. Sun, H. Jin, K. Kaneko, and S. Tazaki, Structure analysis for hole-nuclei close to ^{132}Sn by a large-scale shell-model calculation, Phys. Rev. C **88**, 054310 (2013).

[91] H.-K. Wang, K. Kaneko, and Y. Sun, Quenching of the neutron $N = 82$ shell gap near ^{120}Sr with monopole-driving core excitations, Phys. Rev. C **91**, 021303(R) (2015).

[92] H.-K. Wang, K. Kaneko, Y. Sun, Y. Q. He, S.-F. Li, and J. Li, Monopole effects, isomeric states, and cross-shell excitations in the $A = 129$ hole nuclei near ^{132}Sn, Phys. Rev. C **95**, 011304(R) (2017).

[93] H.-K. Wang, K. Kaneko, and Y. Sun, Isomerism and persistence of the $N = 82$ shell closure in the neutron-rich ^{132}Sn region, Phys. Rev. C **89**, 064311 (2014).

[94] A. Astier, M.-G. Porquet, Ts. Venkova, D. Verney, Ch. Theisen, G. Duchêne, F. Azaiez, G. Barreau, D. Curien, I. Deloncle, O. Dorvaux, B. J. P. Gall, M. Houry, R. Lucas, N. Redon, M. Rousseau, and O. Stézowski, High-spin structures of five N = 82 isotopes: $^{136}_{54}$Xe, $^{137}_{55}$Cs, $^{138}_{56}$Ba, $^{139}_{57}$La, and $^{140}_{58}$Ce, Phys. Rev. C **85**, 064316 (2012).

[95] A. Vogt, M. Siciliano, B. Birkenbach, P. Reiter, K. Hadyńska-Klęk, C. Wheldon, J. J. Valiente-Dobón, E. Teruya, N. Yoshinaga, K. Arnswald, D. Bazzacco, A. Blazhev, A. Bracco, B. Bruyneel, R. S. Chakrawarthy, R. Chapman, D. Cline, L. Corradi, F. C. L. Crespi, M. Cromaz, G. de Angelis, J. Eberth, P. Fallon, E. Farnea, E. Fioretto, C. Fransen, S. J. Freeman, B. Fu, A. Gadea, W. Gelletly, A. Giaz, A. Görgen, A. Gottardo, A. B. Hayes, H. Hess, R. Hetzenegger, R. Hirsch, H. Hua, P. R. John, J. Jolie, A. Jungclaus, V. Karayonchev, L. Kaya, W. Korten, I. Y. Lee, S. Leoni, X. Liang, S. Lunardi, A. O. Macchiavelli, R. Menegazzo, D. Mengoni, C. Michelagnoli, T. Mijatović, G. Montagnoli, D. Montanari, C. Müller-Gatermann, D. Napoli, C. J. Pearson, Zs. Podolyák, G. Pollarolo, A. Pullia, M. Queiser, F. Recchia, P. H. Regan, J.-M. Régis, N. Saed-Samii, E. Şahin, F. Scarlassara, M. Seidlitz, B. Siebeck, G. Sletten, J. F. Smith, P.-A. Söderström, A. M. Stefanini, O. Stezowski, S. Szilner, B. Szpak, R. Teng, C. Ur, D. D. Warner, K. Wolf, C. Y. Wu, and K. O. Zell, High-spin structures in ^{132}Xe and ^{133}Xe and evidence for isomers along the $N = 79$ isotones, Phys. Rev. C **96**, 024321 (2017).

[96] L. Kaya, A. Vogt, P. Reiter, C. Müller-Gatermann, A. Gargano, L. Coraggio, N. Itaco, A. Blazhev, K. Arnswald, D. Bazzacco, B. Birkenbach, A. Bracco, B. Bruyneel, L. Corradi, F. C. L. Crespi, G. de Angelis, M. Droste, J. Eberth, E. Farnea, E. Fioretto, C. Fransen, A. Gadea, A. Giaz, A. Görgen, A. Gottardo, K. Hadyńska-Klęk, H. Hess, R. Hetzenegger, R. Hirsch, P. R. John, J. Jolie, A. Jungclaus, W. Korten, S. Leoni, L. Lewandowski, S. Lunardi, R. Menegazzo, D. Mengoni, C. Michelagnoli, T. Mijatović, G. Montagnoli, D. Montanari, D. Napoli, Zs. Podolyák, G. Pollarolo, F. Recchia, D. Rosiak, N. Saed-Samii, E. Şahin, M. Siciliano, F. Scarlassara, M. Seidlitz, P.-A. Söderström, A. M. Stefanini, O. Stezowski, S. Szilner, B. Szpak, C. Ur, J. J. Valiente-Dobón, M. Weinert, K. Wolf, and K. O. Zell, Identification of high-spin proton configurations in ^{136}Ba and ^{137}Ba, Phys. Rev. C **99**, 014301 (2019).

[97] Samuel M. Harris, Higher order corrections to the cranking model, Phys. Rev. **138**, B509 (1965).

[98] A. Dewald, Transition probabilities in transitional nuclei in the $A = 130$ region, Prog. Part. Nucl. Phys. **28**, 409 (1992).